Vimentin filaments interact with the mitotic cortex allowing normal cell division

Sofia Duarte[1], Álvaro Viedma-Poyatos[1], Elena Navarro-Carrasco[1], Alma E. Martínez[1,a], María A. Pajares[1,2], Dolores Pérez-Sala[1*]

[1]Department of Structural and Chemical Biology, Centro de Investigaciones Biológicas (CSIC), Ramiro de Maeztu 9, 28029 Madrid, Spain.

[2]Molecular Hepatology Group, Instituto de Investigación Sanitaria La Paz (IdiPAZ), Paseo de la Castellana 261, 28046 Madrid, Spain.

Running Title: Novel vimentin-actin interplay in mitosis

Keywords: Vimentin, actin, mitosis, protein-protein interactions, intermediate filaments, HIV, lipoxidation

*To whom correspondence should be addressed at:
Department of Structural and Chemical Biology
Centro de Investigaciones Biológicas
Consejo Superior de Investigaciones Científicas (C.S.I.C.)
Ramiro de Maeztu, 9
28040 Madrid, Spain
Email: dperezsala@cib.csic.es
FAX: 34915360432
Phone: 34918373112

[a]Present address: Centro Cardiologico Monzino, Via Carlo Parea, 4, 20138 Milano MI, Italia

The vimentin network displays remarkable plasticity to support basic cellular functions. Here, we show that in several cell types vimentin filaments redistribute to the cell periphery during mitosis, forming a robust scaffold interwoven with cortical actin. Importantly, the intrinsically disordered tail domain of vimentin is essential for this redistribution, which allows normal mitotic progression. A tailless vimentin mutant forms curly bundles, which remain entangled with dividing chromosomes in mitosis leading to mitotic catastrophes or asymmetric partitions. Serial deletions of the tail domain induce an increasing impairment of cortical association and mitosis progression. Disruption of actin, but not microtubules, mimics the impact of tail deletion. Pathophysiological stimuli, including HIV-protease and lipoxidation, induce similar alterations. Interestingly, filament integrity is not necessary for cortical association, which also occurs in vimentin particles. Taken together, these results unveil novel implications of vimentin dynamics in cell division, in which the tail domain plays a key role.

Introduction

The vimentin filament network provides architectural support for cells and contributes to the positioning and function of cellular organelles [1-3]. Moreover, vimentin plays multiple roles in cell regulation by interacting with signaling proteins, adhesion molecules [4,5], transcription factors [6], chaperones [7,8] and other components of the cytoskeleton [9,10]. The vimentin monomer consists of 466 amino acids organized in a central rod with a predominant α-helical structure flanked by disordered N- and C-terminal domains (Fig. 1A). Vimentin polymerization is believed to progress from parallel dimers, to antiparallel tetramers, eight of which associate laterally in "unit length filaments" that engage head to tail to form filaments. The vimentin network is highly dynamic and rapidly responds to heat shock, oxidative and electrophilic stress, changes in ATP levels and availability of certain divalent cations such as zinc [11-13], thus playing a key role in cell adaptation.

Vimentin filaments can grow at both ends and reportedly exchange subunits along their length. These properties contribute to a fast and versatile network remodeling, in which posttranslational modifications play a key role [14]. Among these, phosphorylation of specific residues regulates vimentin assembly and disassembly into filaments in response to second messengers, as well as its involvement in migration and invasion [15,16]. In mitosis, vimentin phosphorylation is regulated in a spatio-temporal manner, leading to filament disassembly in certain cell types [17,18]. Besides, oxidative and electrophilic modifications of the single vimentin cysteine drastically alter its assembly, suggesting that this residue is critical for filament architecture [13,19].

In addition, vimentin is the substrate for several proteases and the resulting fragments can perform additional roles with impact on cellular functions. Calpains cleave vimentin N-terminus impairing polymerization of the remaining protein structure [20]. In turn, calpain-truncated soluble vimentin species associate with phosphorylated EKR playing a role in axonal regeneration [21], and contribute to the activation of metalloproteases during endothelial cell sprouting [22]. In contrast, amino-terminal fragments generated by caspases during apoptosis exert pro-apoptotic effects [23].

The vimentin C-terminal domain also contains sites for protease cleavage [24], including various viral proteases. Infection with the Moloney mouse sarcoma virus produces a vimentin fragment lacking all or part of the C-terminal tail [25], whereas the HIV-type 1 protease reportedly cleaves vimentin after L423 [26]. In addition, chemicals may promote vimentin cleavage by proteases that remain unidentified. This is the case of gambogic acid, a natural product with anti-inflammatory and anti-tumoral properties, which elicits vimentin cleavage in HeLa cells rendering products missing sequences before S51 and/or after R424 [27].

The role of the tail domain in vimentin organization is still not fully understood, although some insight has been obtained from the study of tail-truncated mutants. Purified tailless vimentin polymerizes in vitro into normal 10 nm-wide filaments [28-30], and presents oligomerization and sedimentation behaviors highly similar to those of full-length vimentin [31]. Nevertheless, under certain polymerization conditions, tailless vimentin filaments display higher heterogeneity, and, in general, a wider average diameter [32]. In turn, the vimentin tail has been suggested to undergo conformational changes during filament elongation and assembly in vitro [33], and to

modulate interactions with divalent cations. In particular, interaction with magnesium has been shown to increase vimentin stiffness in a manner dependent on the presence of the tail domain [34], whereas tailless vimentin has been reported to form bundles thicker than the wt in response to millimolar calcium [28].

In cells, observations on the importance of vimentin tail are highly dependent on the experimental setting. In several vimentin-deficient cell types, tailless vimentin (1-411) forms normal extensive arrays [30], although filaments with a thicker diameter [32] or with a tendency to collapse [29] have been observed. In addition, the vimentin tail has been proposed to act as a cytoplasmic retention signal [35], and certain C-terminal deletion mutants as well as peptides from the N-terminus of vimentin enter the nucleus and induce alterations in nuclear structure [30,36]. Moreover, the C-terminal domain has been reported to contribute to filament stability [29], since its deletion amplified the deleterious effects of several rod mutations on filament assembly in vitro and in cells [29]. However, the mechanism(s) by which C-terminal truncated forms of vimentin could induce cellular perturbations has not been fully elucidated.

As stated above, vimentin is an exquisite sensor for oxidative and electrophilic stress [13]. In the course of studies on vimentin modification by electrophilic lipids (lipoxidation) we have observed that expression of C-terminal truncated mutants, in particular tailless vimentin (1-411) and the reported product of HIV type 1 protease (HIV-PR) cleavage [26], namely, vimentin(1-423), exerted deleterious effects in cells, associated with the formation of juxtanuclear bundles and aberrant mitosis. Searching for the reasons of this toxicity we compared the behavior of full-length and tailless vimentin and found that, if not disassembled, full-length vimentin redistributed to the cell periphery in mitosis, closely interacting with the mitotic cortex and leaving ample space for dividing chromosomes, whereas tailless vimentin snared the mitotic apparatus. These observations suggest an important role of the vimentin tail in network organization and especially in the remodeling taking place during mitosis.

Results

1. Vimentin tail is necessary for appropriate network formation.

The vimentin tail domain can participate in metal binding, filament assembly and stress responses; nevertheless, the precise mechanisms involved are not completely understood. To get insight into these roles, we assessed the organization of tailless vimentin (residues 1-411). Vimentin-deficient SW13/cl.2 cells were cotransfected with bicistronic plasmids coding for untagged vimentin and DsRed as separate products (RFP//vimentin), plus a small amount of GFP-vimentin to light-up the distribution of the network in live cells (Fig. 1A). Under these conditions, vimentin wt formed a normal network. Strikingly, the organization of tailless vimentin was drastically altered, forming thick curly bundles preferentially located at the center of the cell. Expression of tailless vimentin in the vimentin-deficient breast carcinoma cell line MCF7 also led to the formation of coiled bundles (Fig. 1A, lower panels). Therefore, lack of vimentin tail still allows formation of filamentous structures, indicating that its polymerization is not impeded, although its cellular organization is severely altered.

Next, we assessed whether tailless vimentin was able to integrate into filaments formed by vimentin wt or if it disrupted the normal network. For this, variable proportions of vimentin wt and tailless were expressed in SW13/cl.2 cells, as detailed in Fig 1C. We observed that vimentin(1-411) incorporated into filaments of normal appearance when transfected at a low proportion with respect to vimentin wt (8:2, wt:tailless). However, expression of higher proportions of vimentin(1-411) (4:6 or 2:8, wt:tailless) impeded network extension and caused the formation of coiled vimentin bundles (Fig. 1C, lower panels). Moreover, overexpression of vimentin(1-411) but not vimentin wt, in human U373MG astrocytoma cells altered the distribution of endogenous vimentin, leading to its perinuclear condensation (Fig. 1D). This was evidenced by immunofluorescence with anti-vimentin V9, which is directed towards the tail segment, and therefore does not recognize transfected vimentin(1-411) (Supp Fig 1). The proportion of the cytoplasmic area covered by full-length vimentin under both conditions is quantitated in Figure 1E, providing an index of the "collapse" of endogenous vimentin induced by transfection of vimentin(1-411). Thus, tailless vimentin not only shows a severe defect in cellular distribution, but exerts deleterious effects on the organization of full-length vimentin, which depend on the proportion of both forms.

2. Tailless vimentin closely associates with nuclear structures in resting cells and interferes with chromosomes in mitosis.

A more detailed characterization of the distribution of vimentin(1-411) was performed by immunofluorescence with antibodies anti-vimentin N-terminus. Thus, while vimentin wt showed a mostly cytoplasmic localization extending outwards from the nuclear periphery, vimentin(1-411) thick bundles or accumulations were adjacent to the nucleus (Fig. 2A). Curiously, in some cases, these curly bundles showed extensions into the area covered by DAPI staining. Indeed, in cells transfected with CFP-lamin A to delimit the nuclear lamina, vimentin(1-411) appeared in deep invaginations of the nuclear envelope or distributed in the space between nuclear lobules (Fig. 2A, lower panels). These observations were confirmed in live cells co-transfected with the combination of RFP//vimentin and GFP-vimentin to trace vimentin filaments, plus CFP-lamin A (Fig. 2A, right panels). This striking distribution encouraged us to assess the behavior of vimentin(1-411) in mitotic cells. Vimentin organization in mitosis is cell-type dependent, since it can undergo disassembly adopting a diffuse distribution or remain in filamentous structures around the mitotic apparatus [17,37]. In SW13/cl.2 cells vimentin wt was not disassembled in mitosis, but remained in filaments that adopted a marked peripheral distribution (Fig. 2B, upper panels). In fact, 3D reconstruction showed robust vimentin filaments forming a "basket" around dividing chromosomes. In sharp contrast, tailless vimentin remained tightly packed in coiled bundles, frequently in close proximity of condensed chromosomes or forming loops encircling them (Fig. 2B, lower panels).

3. Expression of tailless vimentin leads to aberrant mitosis

As we suspected that vimentin(1-411) could exert deleterious effects, we monitored its fate in live cells. Time-lapse experiments using SW13/cl.2 cells transfected with a combination of RFP//vimentin plus GFP-vimentin wt or (1-411), showed that cells expressing vimentin wt divided regularly, with an interval between cell rounding and separation of daughter cells of 1 to 2 h (Fig. 3A, upper panels). Moreover, vimentin wt was distributed between daughter cells

during cytokinesis. Conversely, cells transfected with tailless vimentin showed persistent bundles that did not loosen during mitosis. Moreover, these cells suffered diverse mitotic perturbations. Some cells attempted to divide for several hours and died during or shortly after mitosis, showing features typical of mitotic catastrophe, like extensive membrane blebbing (Fig. 3A, middle panels). Interestingly, some cells successfully completed division through the asymmetric partitioning of vimentin, implying that tailless vimentin was retained in one of the cells, whereas the other was "rejuvenated", that is, initially free of vimentin coils (Fig. 3A, lower panels). These findings, which are schematically summarized in Fig. 9, show that the tail domain is necessary for normal vimentin dynamics during mitosis.

4. Vimentin localizes to the actomyosin cortex in mitosis and this interaction is impaired in vimentin(1-411).

Vimentin filaments maintain a close crosstalk with other cytoskeletal structures, namely, microtubules and microfilaments, which influence vimentin distribution. Thus, we assessed the interplay of vimentin wt and (1-411) with tubulin and actin. Vimentin wt partially colocalized with tubulin in resting cells (Fig. 4A, upper left). In dividing cells, the two proteins diverged with tubulin concentrating at the mitotic spindle and vimentin lining the cell periphery as shown above. Vimentin(1-411) bundles were largely unconnected to microtubules in resting cells. However, in dividing cells they remained adjacent to the mitotic spindle, in some cases interfering with the position of chromosomes or microtubules (Fig. 4A, left, lower panels). Acute disruption of microtubules with nocodazole under conditions that completely blocked the formation of the mitotic spindle and caused misorientation of chromosomes did not alter the typical peripheral distribution of vimentin wt in mitotic cells (Fig. 4A, right panels). Vimentin(1-411) bundles persisted under these conditions and their distribution in mitotic cells was not drastically altered by nocodazole treatment (Fig. 4A, right, lower panels).

Vimentin has been reported to interact with actin in various ways in interphase cells [9,38,39]. Nevertheless, the vimentin-actin interaction in mitosis has not been previously explored. In mitotic cells, f-actin is known to accumulate at the cell periphery forming, along with myosin, the mitotic actomyosin cortex. This stiff structure protects cells during mitosis, allows spindle formation and orientation, and provides tension which in combination with osmotic pressure maintains the cells spherical shape [40,41]. As illustrated in Fig. 4B, in interphase SW13/cl.2 cells vimentin wt shows little coincidence with f-actin. Interestingly, in mitotic cells, peripherally distributed vimentin appears to line the internal surface of the actomyosin cortex showing points of colocalization with actin, which are clearly evidenced in the fluorescence intensity profiles (Fig. 4B). In sharp contrast, vimentin(1-411) did not follow the actin pattern under any condition. Next, we assessed this distribution in other cell types. In vimentin-deficient MCF7 cells, transfected vimentin showed signs of disassembly in mitosis, with the appearance of amorphous aggregates and some filamentous structures that exhibited limited cortical association (Fig. 4C). In contrast, in U373-MG astrocytoma cells and bovine aortic endothelial cells (BAEC), filamentous structures of endogenous vimentin could be detected that adopted a peripheral distribution, close to the actin cortex (Fig. 4C). Interestingly, in primary dermal fibroblasts from an adult donor (AG10803), a rim of cortical vimentin is observed together with broad loose vimentin bundles that occupy the cytoplasm but do not interfere with chromosomes. These patterns are highlighted in the insets in Fig. 4C, which show enlarged

areas of the cell periphery. Moreover, this distribution is shown in more detail in Supp. Fig. 2, which depicts single channel and merged images, along with the fluorescence intensity profiles for actin and vimentin. Therefore, cortical distribution of vimentin in mitosis appears to be cell-type dependent.

5. Vimentin is intimately intertwined with actin at the mitotic cortex.

To visualize the interaction between vimentin and the mitotic actin cortex in more detail, we employed superresolution microscopy (STED) (Fig. 5A). This confirmed that vimentin filaments were in close proximity of the inner layer of the actin cortex, intermingled with actin at some points (Fig. 5A, upper row) or running between two actin layers, as clearly shown by the co-localization mask (Figure 5A, second row from the top). Actin-vimentin co-localization analysis indicated that this close connection was not continuous but occurred at certain locations along the mitotic cortex, suggesting that there may be sites of anchorage for vimentin in this structure. Three-dimensional reconstructions shed light on this interaction by revealing the robust basket-shaped vimentin framework (Fig. 5B). This net-like organization of vimentin clarifies why in some single sections only “arcs” or discrete signals of vimentin are detected, depending on the orientation of the filaments, which interacting with the cortex at some points. In the arcs the degree of co-localization was quite significant, as depicted in Fig. 5A (insets). In contrast, the distribution of actin appeared much more uniform along the mitotic cortex, forming a hollow sphere. This can be appreciated in the three-dimensional reconstruction of the bottom half of the cell depicted in Figure 5C. Interestingly, actin distribution shows a reduced density at some places, coinciding with the position of vimentin bundles (marked by an arrowhead in Fig. 5C). Indeed, observation of the exterior of the sphere evidences points at which vimentin filaments impinge the overlaying actin cortex (marked by arrows in Fig. 5C).

6. Vimentin cortical localization in mitosis is impaired by actin disruption and pathophysiological stimuli

To explore a putative role of filamentous actin (f-actin) in vimentin peripheral localization, we used several strategies to disrupt actin polymerization (Fig. 6). Cytochalasin B elicited a patchy f-actin distribution, whereas vimentin organization was not severely affected in most resting cells (Fig. 6A). However, in cytochalasin B-treated mitotic cells vimentin wt appeared in bundles and remained entangled with dividing chromosomes, resembling vimentin(1-411), the distribution of which was not further altered by cytochalasin B. Latrunculin A induced a marked decrease in the intensity of Phalloidin staining, with the little f-actin remaining distributing in scattered aggregates (Fig. 6B). Loss of f-actin in mitosis correlated with the formation of vimentin bundles intertwined with dividing chromosomes. Rho proteins are involved in the assembly of the actomyosin cortex in mitosis [42], and in particular RhoA is important for the cortical enrichment of f-actin and the assembly of myosin II [43]. Interestingly, treatment with C3 toxin to inhibit Rho proteins resulted in a less homogeneous actin cortex and compromised the peripheral distribution of vimentin in mitotic cells. The myosin II ATPase inhibitor blebbistatin induced intense shrinking of the cell margins giving the cells a “branched” appearance (Fig. 6B), as previously observed [44,45]. Thus, in non-dividing cells, blebbistatin led to a more thorny/spiky appearance of actin whereas vimentin was condensed

at the cytoplasmic "branches". In mitotic cells, the actin cortex was less homogeneous and vimentin could also be observed at the central region of the cell, although these alterations seemed milder than those elicited by actin-disrupting agents (Fig. 6B). Thus, of different cytoskeletal proteins, our observations point to a predominant role of actin in vimentin redistribution in mitosis, which requires the presence of the tail domain.

Next, we assessed whether pathophysiological agents known to cause vimentin "collapse" altered its distribution in mitosis. The inflammatory lipid mediators 2-hydroxynonenal and prostaglandin A_1, caused a juxtanuclear condensation of vimentin in interphase cells, consistent with previous observations [13]. Moreover, they significantly dislodged vimentin from the acto-myosin cortex in mitosis (Fig. 6C). This effect was quantitated by calculating the ratio between central and total vimentin fluorescence in mitotic cells (Fig. 6C, lower graph). Nevertheless, under these conditions, lipoxidative damage to molecules other than vimentin can contribute to this effect. In addition, we explored the impact of viral protease cleavage by co-transfecting SW13/cl.2 cells with an expression vector for HIV protease (GFP-PR) along with RFP//vimentin wt plus a tracer amount of mCherry-vimentin to monitor live cells (Fig. 6D). Protease expression, indicated by the green cytoplasmic fluorescence (Fig. 6D, insets), was associated with collapse of vimentin filaments into curly juxtanuclear bundles or accumulations, reminiscent of the distribution of vimentin(1-411). Vimentin collapse was blocked by the reversible HIV-PR inhibitor ritonavir, whereas its withdrawal allowed fast condensation of vimentin, indicating that this was due to protease cleavage (Fig. 6D, lower panels). Vimentin accumulations were not resolved in mitosis and concentrated close to the dividing chromosomes (Fig. 6E). Nevertheless, it should be taken into account that electrophilic lipids as well as HIV-PR-induced vimentin alterations could occur through both direct and indirect mechanisms. Nonetheless, these results show that various pathophysiological stimuli cause anomalous distribution of vimentin in mitosis, hampering cortical localization.

7. Impact of serial C-terminal deletions on vimentin organization and peripheral distribution in mitosis

To define more precisely the region determining vimentin peripheral localization in mitosis, we explored the distribution of vimentin mutants bearing several C-terminal deletions (Fig. 7A). As HIV-type I protease has been reported to cleave vimentin at Leu423 [26,46,47], we first generated a vimentin(1-423) construct, and assessed its distribution and effects in cells. As shown in Figure 7B, vimentin-deficient cells, including SW13/cl.2 and MCF7 cells, transfected with the combination of RFP//vimentin(1-423) and GFP-vimentin(1-423) for live observation, displayed complex curly bundles located in the proximity of the nucleus, similar to the structures formed by vimentin(1-411). Vimentin(1-423) coiled bundles did not redistribute to the cell periphery in mitosis but remained next to the condensed chromosomes, either interfering with the mitotic spindle or located at one of the poles (Fig. 7C). Other alterations included the frequent appearance of bi- or multi-nucleated cells that contained coiled vimentin, and in some cases DNA, in the space between nuclei, indicative of cytokinetic defects. Time-lapse monitoring showed that cells expressing vimentin(1-423) displayed marked alterations of mitosis analogous to those observed for vimentin(1-411), including asymmetric partitioning of

vimentin, delayed mitosis and cell death (Fig. 7D). Moreover, actin staining showed lack of cortical association of vimentin(1-423) in mitotic cells (Fig. 7E).

Vimentin(1-448), preserving fifteen amino acids more (Fig. 7A), yielded a heterogeneous pattern where both extended filaments and robust bundles or accumulations could be observed by several transfection and visualization strategies (Fig. 7F). In mitosis, cells bearing this vimentin form frequently showed bundles, although they often appeared at basal planes or at the cell periphery (Fig. 7G). The fate of mitotic cells showed two main patterns (Fig. 7H). Approximately 40% showed delayed separation ending in cell death, indicative of cytokinetic failure, whereas 60% of the cells completed mitosis, although with asymmetric partition of vimentin. Moreover, it was also possible to detect some peripheral filamentous vimentin, which actin staining confirmed to lie adjacent to the actomyosin cortex (Fig 7I).

Finally, the consequences of a shorter C-terminal deletion eliminating residues 460 to 466 were explored. RFP//vimentin(1-459) formed filaments of morphology and extension similar to those of vimentin wt, although small bundles or curls were also observed in approximately 18 % of the cells (Fig. 7J). Live cells transfected with RFP//vimentin(1-459) plus GFP-vimentin(1-459) showed a similar pattern (Fig. 7J, right panel). In mitotic cells, vimentin(1-459) adopted a mainly peripheral distribution, although some cells presented filaments intertwined with chromosomes (Fig. 7K). Live monitoring of mitosis (Fig. 7L) showed two different patterns: cells lacking vimentin bundles underwent basically normal mitosis with even vimentin distribution between daughter cells (upper panels); cells harboring vimentin bundles showed a partially asymmetric distribution of vimentin content, with both daughter cells receiving vimentin but one of them in a small proportion (fig. 7L, lower panels, arrows) and the other retaining the bundle. Actin staining showed coincidence of vimentin with some segments of the actin cortex in mitotic cells accompanied by persistence of some filaments in the central area, as depicted in the fluorescence profiles (Fig. 7M). These results indicate a mild perturbation of vimentin distribution during mitosis by deletion of the last seven amino acids.

Taken together, these results indicate that step-wise deletion of the vimentin tail gradually impairs normal vimentin assembly and redistribution in mitosis, with the most drastic effects being observed upon truncation at Leu423 or I411, which completely abolish the peripheral localization of vimentin in mitotic cells.

8. Vimentin cortical association in mitosis does not require network formation or full filament assembly

To discard the possibility that lack of cortical association could be due to intense bundling, we used GFP-vimentin fusion constructs, which do not form full filaments in SW13/cl.2 cells, and show a disperse distribution throughout the cytoplasm [13]. Thus, we studied the organization of GFP-vimentin wt and all the truncated variants (Fig. 8A). GFP-vimentin wt formed a uniform lattice of squiggles or short filaments [13] (Fig 8A). In contrast, GFP-vimentin(1-411) could not reach the squiggle stage and formed only bright dots, thus highlighting the elongation defect of this mutant. GFP-vimentin(1-423) gave rise to a mixed pattern consisting of dots, small swirls and occasional short filaments. Similarly, GFP-vimentin(1-448) formed mainly bright dots, with short filaments or swirls appearing in approximately 30% of the cells, and this proportion was higher for the GFP-vimentin(1-459) construct. A quantitation of the proportion

of cells presenting squiggles or short filaments is given in the graph shown in Fig. 8A, right panel. Thus, the use of GFP-fusion constructs in vimentin-deficient cells confirms a gradual sequence-dependent impairment of particle elongation, highlighting that even small truncations of the tail domain have a detectable impact in this model.

Next, we explored the localization of the various GFP-fusion constructs with respect to actin. The pattern observed in resting cells is shown in the left panel for every construct (Fig. 8B). Most constructs showed little overlap with actin structures in resting cells, with GFP-vimentin wt, C328S and (1-459) displaying more points of contact. Nevertheless, we focused on the distribution of these constructs in cells arrested in mitosis by mild nocodazole treatment (Fig. 8B, right panels and profiles). In mitotic cells, GFP-vimentin constructs frequently showed a diffuse green background, suggesting that they disassemble to a higher extent that untagged vimentin. Nevertheless, GFP-vimentin wt structures could be clearly detected in the proximity of the cell cortex in mitosis showing co-localization with actin (Fig. 8B). In sharp contrast, GFP-vimentin(1-411) appeared as dots scattered throughout the cell. Importantly, lack of cortical association cannot be solely attributed to defective elongation since dots formed by another elongation-incompetent construct, namely, full length GFP-vimentin C328S [13], effectively relocated to the periphery of mitotic cells (Fig 8B). Interestingly, GFP-vimentin(1-423) accumulations also failed to associate with the actin cortex, whereas more than 60% of GFP-vimentin(1-448) dots were located at the cell periphery. The proportion of dots from the various constructs that show cortical localization is summarized in the histogram depicted in Fig. 8C, bottom panel. Moreover, cortical localization of GFP-vimentin(1-459) mixed structures was preserved. Taken together, these observations illustrate the graded impact of vimentin tail truncation on cortical association in mitosis and point to the importance of the segment comprised between amino acids 424 and 448 for this redistribution (Fig. 8D). Furthermore, they show that full filament elongation is not necessary for cortical association since vimentin particles formed by constructs retaining most of the tail domain, effectively relocate to the cell periphery.

Taken together, these results indicate that, at least in several cell types in which vimentin is not disassembled in mitosis, the tail domain is necessary for peripheral localization of the protein. This redistribution towards the mitotic cortex avoids vimentin accumulation close to the mitotic spindle, which hampers mitosis. Importantly, cortical localization does not require full filament assembly or network formation.

Discussion

Vimentin plays critical functions in cell mechanics [48]. Vimentin exists in cells in several assembly forms, the exact organization of which is not totally understood. In particular, the disposition of the intrinsically disordered head and tail domains remains an intriguing problem. Here, we found a striking distribution of tailless vimentin (residues 1-411), characterized by intense juxtanuclear bundling and severe mitotic alterations, including asymmetric partitions and mitotic catastrophes. This drove us to pursue the behavior of full-length vimentin, therefore unveiling the robust scaffold formed by vimentin in mitosis in several cell types, in which it does not disassemble. The vimentin mitotic framework closely interacts with the

actomyosin cortex, and intertwines with actin, thus appearing to cling to and/or support this structure. From our observations, two functions can be hypothesized for this arrangement: to yield space for the division of chromosomes to take place and, potentially, to give robustness to the mitotic cortex.

The distribution of vimentin in mitosis appears to respond to two main patterns: in some cells, vimentin filaments form a “cage” surrounding the mitotic spindle, whereas in others, phosphorylation in combination with protein-protein interactions, namely with nestin, leads to filament disassembly [17]. Among phosphorylation sites, those located at the N-terminus of the protein, namely S55, have been attributed a key role in vimentin disassembly in mitosis [49], with sites at the C-terminal (T457, S458) playing no obvious role [17], although their involvement cannot be excluded. Here, we have employed a variety of cell types allowing analysis of vimentin behavior in several settings. Among cancer cell lines, vimentin remains as a robust scaffold in transfected SW13/cl.2 cells, which are nestin-deficient. In contrast, partial vimentin disassembly and poor association with the actin cortex are observed in mitotic MCF7 cells, which express nestin [50]. In U373-MG astrocytoma cells, which may express variable proportions of nestin and vimentin [51], and BAEC, which express nestin in culture, both, areas of disassembly and of cortical enrichment can be found. Curiously, in mitotic human dermal fibroblasts, vimentin forms broad bundles in the cytoplasm but a rim of vimentin close to the actin cortex can be observed. Thus, in several relevant cell types, cortical association of vimentin filaments with the mitotic cortex is significant. Nevertheless, this distribution has not been studied previously.

Our results show that the C-terminal domain is essential for the formation of an extended vimentin filament network and for the cortical association of vimentin filaments in mitosis. This segment of unknown structure has been proposed to suffer important conformational alterations during filament assembly and to participate in protein-protein interactions, i.e. with actin. Indeed, actin has been reported to influence vimentin polymerization in vitro in a manner dependent on the presence of the C-terminal tail [52]. Moreover, a peptide from vimentin tail has been show to associate with actin when microinjected in *Xenopus* A6 cells [53].

In resting cells, a complex interplay between vimentin and actin at several levels of organization can take place. [54]. Actin has been shown to limit the transport of vimentin ULF along microtubules [55], whereas vimentin reportedly restrains actin polymerization. In fact, vimentin depletion activates GEF-H1, RhoA and actin stress fiber assembly [39]. This bidirectional interplay appears to be particularly relevant at actomyosin arcs, which have been described to interact with vimentin filaments through the scaffold protein plectin, and drive their retrograde movement, thus promoting vimentin perinuclear localization [38]. In turn, vimentin restricts retrograde movement of the arcs. Nevertheless, the interaction of actin and vimentin in mitosis, to the best of our knowledge, has not been addressed.

Our results indicate that in mitosis, filamentous vimentin is located very close to the actomyosin cortex showing points of interaction, as observed by superresolution microscopy. Nevertheless, this interaction could be indirect, and involve other proteins present at the cortex or at the plasma membrane or even lipids. A reasonable candidate to mediate this interaction is the scaffold protein plectin [56]. Nevertheless, the distribution of plectin in mitosis

is not well characterized and both, solubilization and dissociation from vimentin [57], as well as preservation of partial association [58], have been documented in different cell types. Also, since vimentin surpasses the actomyosin cortex at some points, sites of attachment at the plasma membrane involving protein receptors or lipid domains, cannot be excluded. Nonetheless, our results show that cortical association of vimentin requires integrity of the actomyosin cortex, as several strategies that interfere with actin polymerization compromise the peripheral distribution of vimentin in dividing cells. In contrast, disruption of microtubules does not seem to affect vimentin peripheral redistribution. Moreover, dislodgement of vimentin from the cell periphery can also be caused by several pathophysiological agents inducing vimentin disruption, including lipid electrophiles and HIV-protease. In this context, several proteases activated during stress or viral infections have been reported to cleave the C-terminal domain of vimentin [25,26], which also contains consensus sites for other proteases, such as cathepsin K, calpain or certain metalloproteases, according to the protease specific prediction server PROSPER (https://prosper.erc.monash.edu.au). As tailless vimentin is able to disrupt full length vimentin if reaching a similar proportion, the functional consequences of the cleavage could be fatal when cells attempt to divide. In this vein, the deleterious effect of the absence of the tail domain would be more significant in cells in which vimentin retains its filamentous structure during mitosis. Nonetheless, it should be taken into account that the effect of vimentin disrupting agents and proteases could be due to alteration not only of vimentin but of other cellular structures, including actin.

In this study we have used tail-truncated mutants of vimentin, both as untagged proteins and as GFP-fusion constructs. We have previously shown that GFP fusion constructs of vimentin undergo incomplete elongation and display more intense perturbations that untagged vimentin upon stress or certain mutations [13]. Notably, these constructs also evidenced a progressive alteration of elongation upon elimination of increasing tail segments, with shorter constructs forming mainly dots and those with milder truncations showing an increasing proportion of squiggles or short filaments. Importantly, both untagged and GFP-fusion constructs showed a graded impairment of cortical association upon serial deletions of the tail, with the strongest impact occurring after deletion of the 43 distal amino acids, since vimentin(1-448) constructs preserve some cortical association. Therefore, the sequence comprised between amino acids 424 and 448 appears to contain important determinants for redistribution to the mitotic cortex. The conformation of this region in the context of the filaments or even the tetramers of vimentin is not known. Nevertheless, several lines of indirect evidence suggest that the tail could fold back onto the distal segment of the rod forming a loop that would protrude from filaments, providing a support for protein-protein interactions [59,60]. Although this contention still needs conclusive experimental evidence, the sequence forming this loop would approximately coincide with the 424-448 segment. Nevertheless, our observations on the distribution of elongation-defective constructs, like GFP-vimentin C328S, show that organization of vimentin into full filament structures is not necessary for cortical localization, since vimentin dots formed by the GFP-vimentin C328S mutant effectively associate with the cell periphery.

Concluding remarks

In summary, we have observed that, if not disassembled, vimentin filaments redistribute to the cell periphery in mitosis, closely interacting with the actomyosin cortex, thus unveiling a novel feature of intermediate filament dynamics during the cell cycle. This reorganization requires the tail domain of vimentin and is important for mitosis to proceed normally. Thus, pathophysiological processes affecting the integrity of vimentin tail in a sufficient proportion may have deleterious consequences for cell proliferation. Therefore, our results provide the first proof that vimentin tail facilitates its association with the actin cortex in mitosis. Moreover, they open the way to search for strategies modulating these interactions.

Materials and methods

Reagents. Restriction enzymes and buffers were from Promega. Anti-vimentin antibodies were: mouse monoclonal V9 clone (sc-6260) and its Alexa-488 conjugate from Santa Cruz Biotechnology, mouse anti-vimentin monoclonal antibody from Sigma, rabbit anti-human vimentin C-terminal antibody from RayBiotech and anti-human vimentin clone VIM 3B4 from Millipore. Anti-actin was from Sigma and anti-α-tubulin from Abcam. Anti-GFP was from Roche. C3 transferase toxin was from Cytoskeleton. Latrunculin A was from Santa Cruz Biotechnology. 4-hydroxynonenal (HNE) and prostaglandin A_1 (PGA_1) were from Cayman Chemical. 4,6-diamidino-2-phenylindole (DAPI), blebbistatin and ritonavir were from Sigma.

Cell culture and treatments. SW13/cl.2 vimentin-deficient cells were the generous gift of Dr. A. Sarriá (University of Zaragoza, Spain)[61]. Breast carcinoma MCF7 and U373-MG human glioblastoma astrocytoma cells were from ATCC. They were cultured in DMEM with 10% (v/v) fetal bovine serum (FBS) and antibiotics (100 U/ml penicillin and 100 μg/ml streptomycin). Bovine aortic endothelial cells (BAEC) were from Clonetics and were cultured in RPMI1640 supplemented with 10% (v/v) newborn calf serum (Gibco) and antibiotics. Primary human dermal fibroblasts (ref. AG10803) were obtained from the NIA Aging Cell Repository at the Coriell Institute for Medical Research (Camden, NJ). Unless otherwise stated, treatments were carried out in serum-free medium. For acute microtubule disruption, cells were treated with 5 μM nocodazole for 30 min. For mitotic arrest, cells were cultured in the presence of 0.4 μM nocodazole for 20 h in complete medium. This treatment was employed, when indicated, to increase the proportion of mitotic cells in conditions under which neither actin, nor vimentin organization were altered with respect to untreated cells (Suppl. Fig. 3). Disruption of filamentous actin (f-actin) was achieved by treatment with 10 μM cytochalasin B or 2.5 μM latrunculin A for 30 min, or 2 μg/ml C3 toxin for 3.5 h. Blebbistatin was used at 20 μM for 1 h. For treatment with electrophilic lipids cells were incubated in the presence of 10 μM HNE for 4 h, or 20 μM PGA_1 for 20 h. Inhibition of transfected HIV protease was achieved by incubating the cells in the presence of 10 μM ritonavir in serum-containing medium, immediately after transfection. For removal of the inhibitor cells were washed three times with fresh medium with serum but without antibiotics.

Plasmids and transfections. The bicistronic plasmid coding for the red fluorescent protein (DsRed Express2) and wt human vimentin as separate products, RFP//vimentin wt, and the

GFP fusion constructs, GFP-vimentin wt and GFP-vimentin C328S have been previously described [13,62]. The various tail truncated mutants, vimentin (1-145), (1-411), (1-423) and (1-459) were generated introducing stop codons at positions 146, 412, 424, 449 and 460, respectively, by site directed mutagenesis of the parent vectors using the Quikchange XL mutagenesis kit from Stratagene and the primers specified in Table 1, following the instructions of the manufacturer. Truncated vimentin constructs showed the expected mobility in SDS-PAGE gels as well as immunoreactivity (Suppl. Fig. 5). Thus, all constructs used were recognized by an antibody raised against full-length vimentin, which recognizes the N-terminus of the protein (anti-vim N-term), whereas an antibody against the beginning of the tail (clone V9) recognized all constructs except tailless vimentin (1-411). The CFP-lamin A plasmid was the gift of Dr. Vicente Andrés [63]. The vector encoding HIV type I protease in fusion with GFP (pcDNA3/GFP-PR) described in [64] was a gift from Nico Dantuma (Addgene plasmid #20253). Cells were transfected using Lipofectamine 2000 (Thermo Scientific), as previously described [13,65]. Routinely, cells were visualized 48 h after transient transfection. When indicated, cells were cultured in the presence of G-418 at 500 μg/ml for generation of stably transfected cells.

Fluorescence microscopy. Cells transfected with the various constructs were visualized live by confocal microscopy on Leica SP2 or SP5 microscopes. Images were acquired every 0.5 μm and single sections or overall projections are shown, as indicated. For immunofluorescence, cells were fixed with 4% (w/v) paraformaldehyde for 25 min at r.t., permeabilized with 0.1% Triton-X100 (v/v) in PBS and blocked with 1% (w/v) BSA in PBS. Antibodies were used at 1:200 dilution in blocking solution. Filamentous actin was stained with Phalloidin-Alexa568 or Phalloidin-Alexa488 (Molecular Probes), following manufacturer instructions. Nuclei were counterstained with DAPI (3 μg/ml). Direct visualization on glass-bottom culture dishes was found optimal for imaging mitotic cells, since mounting on glass slides compromised their spherical shape. For superresolution microscopy through stimulated emission depletion (STED), vimentin was detected with Alexa488-conjugated anti-vimentin V9 and filamentous actin was stained with Phalloidin-Tetramethylrhodamine B isothiocyanate from Sigma (0.5 μg/ml). Images were acquired with a confocal multispectral Leica TCS SP8 system equipped with a 3X STED module. Colocalization was analyzed with Leica software. Time-lapse microscopy was carried out in a multidimensional microscopy system Leica AF6000 LX in a humidified 5% CO_2 atmosphere at 37°C. 3D reconstructions were obtained with Image J or Imaris software. Fluorescence intensity plots and fluorescence intensity measurements were obtained with ImageJ software. For quantitation of vimentin reorganization induced by electrophilic lipids, the proportion of vimentin fluorescence present in the central area of mitotic cells (central circle of a diameter of 60% the total cell diameter), with respect to the total area was measured as an indication of the impairment of peripheral distribution.

SDS-PAGE and western blot. Cells transfected with the various constructs were lysed in 20 mM Tris-HCl pH 7.5, 0.1 mM EDTA, 0.1 mM EGTA, 0.1 mM β-mercaptoethanol, containing 0.5% SDS, 0.1 mM sodium orthovanadate and protease inhibitors (2 μg/ml each of leupeptin, aprotinin and trypsin inhibitor, and 1.3 mM Pefablock), and processed essentially as described[66]. Briefly, protein concentration in lysates was determined by the bicinchoninic acid assay. Aliquots of lysates containing 30 μg of total protein were denatured in Laemmli buffer for 5 min at 95°C and separated in 10 or 15% polyacrylamide gels. Gels were transferred to

Immobilon-P membranes (Millipore) using a Tris-glycine methanol three-buffer system, as recommended by the manufacturer, on a semi-dry transfer unit (Transblot) from Bio-Rad. Membranes were blocked with 2% (w/v) low-fat powdered milk in T-TBS (Tris-HCl pH 7.5, 500 mM NaCl, 0.05% (v/v)Tween-20). Subsequently, membranes were incubated with primary antibodies at 1:500 dilution and horseradish peroxidase-conjugated secondary antibodies (Dako) at 1:2000 dilution. Proteins of interest were detected with the ECL system from GE Healthcare.

Statistical analysis. All experiments were repeated at least three times with similar results. All results are presented as average values ± SEM. Statistical differences were evaluated by the Student's t-test and were considered significant when $P<0.05$, which is denoted in graphs by an asterisk.

Acknowledgements. This work has been funded by the European Union's Horizon 2020 research and innovation program under the Marie Sklowdowska-Curie grant agreement number 675132, "Masstrplan" (http://cordis.europa.eu/project/rcn/ 198275_en.html), and by grants from the Spanish Ministerio de Economía y Competitividad (MINECO/FEDER, http://www.mineco.gob.es/portal/site/mineco/idi) SAF2015-68590R and from Instituto de Salud Carlos III/FEDER, RETIC Aradyal RD16/0006/0021. AVP is supported by the FPI Program from MINECO, reference: BES-2016-076965. Feedback from the COST Action CA15214 "EuroCellNet " is gratefully acknowledged.

We are indebted to MT Seisdedos and Dr. G Elvira from CIB, and Dr. S Gutiérrez from CNB, CSIC for help with confocal and superresolution microscopy, respectively. We thank Dr. Francisco J. Sánchez-Gómez and Prof. F.J. Cañada for helpful comments and discussion. The valuable technical assistance of MJ Carrasco is gratefully appreciated.

References

1 Guo, M. *et al.* Probing the stochastic, motor-driven properties of the cytoplasm using force spectrum microscopy. *Cell* **158**, 822-832, doi:10.1016/j.cell.2014.06.051 (2014).

2 Styers, M. L. *et al.* The endo-lysosomal sorting machinery interacts with the intermediate filament cytoskeleton. *Mol Biol Cell* **15**, 5369-5382, doi:10.1091/mbc.E04-03-0272 (2004).

3 Chernoivanenko, I. S., Matveeva, E. A., Gelfand, V. I., Goldman, R. D. & Minin, A. A. Mitochondrial membrane potential is regulated by vimentin intermediate filaments. *FASEB J* **29**, 820-827, doi:10.1096/fj.14-259903 (2015).

4 Bhattacharya, R. *et al.* Recruitment of vimentin to the cell surface by beta3 integrin and plectin mediates adhesion strength. *J Cell Sci* **122**, 1390-1400, doi:10.1242/jcs.043042 (2009).

5 Kim, J. *et al.* Vimentin filaments regulate integrin-ligand interactions by binding to the cytoplasmic tail of integrin beta3. *J Cell Sci* **129,** 2030-2042, doi:10.1242/jcs.180315 (2016).

6 Tsai, Y. C. *et al.* Cytoskeletal protein vimentin interacts with and regulates peroxisome proliferator-activated receptor gamma via a proteasomal degradation process. *J Cell Biochem* **114**, 1559-1567, doi:10.1002/jcb.24497 (2013).

7 Lee, J. S. *et al.* Heat shock protein 27 interacts with vimentin and prevents insolubilization of vimentin subunits induced by cadmium. *Exp & Mol Med* **37**, 427-435, doi:10.1038/emm.2005.53 (2005).
8 Zhang, M. H. *et al.* HSP90 protects apoptotic cleavage of vimentin in geldanamycin-induced apoptosis. *Mol Cell Biochem* **281**, 111-121, doi:10.1007/s11010-006-0638-x (2006).
9 Chang, L. & Goldman, R. D. Intermediate filaments mediate cytoskeletal crosstalk. *Nat Rev Mol Cell Biol* **5**, 601-613, doi:10.1038/nrm1438 (2004).
10 Kim, H. *et al.* Regulation of cell adhesion to collagen via β1 integrins is dependent on interactions of filamin A with vimentin and protein kinase C epsilon. *Exp Cell Res* **316**, 1829-1844 (2010).
11 de Pablo, Y., Nilsson, M., Pekna, M. & Pekny, M. Intermediate filaments are important for astrocyte response to oxidative stress induced by oxygen-glucose deprivation and reperfusion. *Histochem Cell Biol* **140**, 81-91, doi:10.1007/s00418-013-1110-0 (2013).
12 Robert, A., Rossow, M. J., Hookway, C., Adam, S. A. & Gelfand, V. I. Vimentin filament precursors exchange subunits in an ATP-dependent manner. *Proc Natl Acad Sci U S A* **112**, E3505-3514, doi:10.1073/pnas.1505303112 (2015).
13 Pérez-Sala, D. *et al.* Vimentin filament organization and stress sensing depend on its single cysteine residue and zinc binding. *Nat Commun* **6**, 7287, doi:10.1038/ncomms8287 (2015).
14 Snider, N. T. & Omary, M. B. Post-translational modifications of intermediate filament proteins: mechanisms and functions. *Nat Rev Mol Cell Biol* **15**, 163-177, doi:10.1038/nrm3753 (2014).
15 Sihag, R. K., Inagaki, M., Yamaguchi, T., Shea, T. B. & Pant, H. C. Role of phosphorylation on the structural dynamics and function of types III and IV intermediate filaments. *Exp Cell Res* **313**, 2098-2109, doi:10.1016/j.yexcr.2007.04.010 (2007).
16 Zhu, Q. S. *et al.* Vimentin is a novel AKT1 target mediating motility and invasion. *Oncogene* **30**, 457-470, doi:10.1038/onc.2010.421 (2011).
17 Chou, Y. H., Khuon, S., Herrmann, H. & Goldman, R. D. Nestin promotes the phosphorylation-dependent disassembly of vimentin intermediate filaments during mitosis. *Mol Biol Cell* **14**, 1468-1478, doi:10.1091/mbc.E02-08-0545 (2003).
18 Izawa, I. & Inagaki, M. Regulatory mechanisms and functions of intermediate filaments: a study using site- and phosphorylation state-specific antibodies. *Cancer Sci* **97**, 167-174, doi:10.1111/j.1349-7006.2006.00161.x (2006).
19 Mohan, R. & Bargagna-Mohan, P. The Use of Withaferin A to Study Intermediate Filaments. *Methods Enzymol* **568**, 187-218, doi:10.1016/bs.mie.2015.09.025 (2016).
20 Traub, P. & Vorgias, C. E. Involvement of the N-terminal polypeptide of vimentin in the formation of intermediate filaments. *J Cell Sci* **63**, 43-67 (1983).
21 Perlson, E. *et al.* Vimentin-dependent spatial translocation of an activated MAP kinase in injured nerve. *Neuron* **45**, 715-726, doi:10.1016/j.neuron.2005.01.023 (2005).
22 Kwak, H. I. *et al.* Calpain-mediated vimentin cleavage occurs upstream of MT1-MMP membrane translocation to facilitate endothelial sprout initiation. *Angiogenesis* **15**, 287-303, doi:10.1007/s10456-012-9262-4 (2012).
23 Byun, Y. *et al.* Caspase cleavage of vimentin disrupts intermediate filaments and promotes apoptosis. *Cell Death Differ* **8**, 443-450, doi:10.1038/sj.cdd.4400840 (2001).
24 Fischer, S., Vandekerckhove, J., Ampe, C., Traub, P. & Weber, K. Protein-chemical identification of the major cleavage sites of the Ca2+ proteinase on murine vimentin, the mesenchymal intermediate filament protein. *Biol Chem Hoppe-Seyler* **367**, 1147-1152 (1986).

25 Singh, B. & Arlinghaus, R. B. Vimentin phosphorylation by p37mos protein kinase in vitro and generation of a 50-kDa cleavage product in v-mos-transformed cells. *Virology* **173**, 144-156 (1989).
26 Shoeman, R. L. *et al.* Human immunodeficiency virus type 1 protease cleaves the intermediate filament proteins vimentin, desmin, and glial fibrillary acidic protein. *Proc Natl Acad Sci U S A* **87**, 6336-6340 (1990).
27 Yue, Q. *et al.* Proteomic Analysis Revealed the Important Role of Vimentin in Human Cervical Carcinoma HeLa Cells Treated With Gambogic Acid. *Mol Cell Proteomics* **15**, 26-44, doi:10.1074/mcp.M115.053272 (2016).
28 Eckelt, A., Herrmann, H. & Franke, W. W. Assembly of a tail-less mutant of the intermediate filament protein, vimentin, in vitro and in vivo. *Eur J Cell Biol* **58**, 319-330 (1992).
29 McCormick, M. B., Kouklis, P., Syder, A. & Fuchs, E. The roles of the rod end and the tail in vimentin IF assembly and IF network formation. *J Cell Biol* **122**, 395-407 (1993).
30 Rogers, K. R. *et al.* Truncation mutagenesis of the non-alpha-helical carboxyterminal tail domain of vimentin reveals contributions to cellular localization but not to filament assembly. *Eur J Cell Biol* **66**, 136-150 (1995).
31 Mucke, N. *et al.* Molecular and biophysical characterization of assembly-starter units of human vimentin. *J Mol Biol* **340**, 97-114, doi:10.1016/j.jmb.2004.04.039 (2004).
32 Herrmann, H. *et al.* Structure and assembly properties of the intermediate filament protein vimentin: the role of its head, rod and tail domains. *J Mol Biol* **264**, 933-953, doi:10.1006/jmbi.1996.0688 (1996).
33 Hess, J. F., Budamagunta, M. S., Aziz, A., FitzGerald, P. G. & Voss, J. C. Electron paramagnetic resonance analysis of the vimentin tail domain reveals points of order in a largely disordered region and conformational adaptation upon filament assembly. *Protein Sci* **22**, 47-55, doi:10.1002/pro.2182 (2013).
34 Lin, Y. C. *et al.* Divalent cations crosslink vimentin intermediate filament tail domains to regulate network mechanics. *J Mol Biol* **399**, 637-644, doi:10.1016/j.jmb.2010.04.054 (2010).
35 Lowrie, D. J., Jr., Stickney, J. T. & Ip, W. Properties of the nonhelical end domains of vimentin suggest a role in maintaining intermediate filament network structure. *J Struct Biol* **132**, 83-94, doi:10.1006/jsbi.2000.4315 (2000).
36 Shoeman, R. L., Huttermann, C., Hartig, R. & Traub, P. Amino-terminal polypeptides of vimentin are responsible for the changes in nuclear architecture associated with human immunodeficiency virus type 1 protease activity in tissue culture cells. *Mol Biol Cell* **12**, 143-154 (2001).
37 Djabali, K., Piron, G., de Nechaud, B. & Portier, M. M. alphaB-crystallin interacts with cytoplasmic intermediate filament bundles during mitosis. *Exp Cell Res* **253**, 649-662, doi:10.1006/excr.1999.4679 (1999).
38 Jiu, Y. *et al.* Bidirectional Interplay between Vimentin Intermediate Filaments and Contractile Actin Stress Fibers. *Cell reports* **11**, 1511-1518, doi:10.1016/j.celrep.2015.05.008 (2015).
39 Jiu, Y. *et al.* Vimentin intermediate filaments control actin stress fiber assembly through GEF-H1 and RhoA. *J Cell Sci* **130**, 892-902, doi:10.1242/jcs.196881 (2017).
40 Kunda, P. & Baum, B. The actin cytoskeleton in spindle assembly and positioning. *Trends Cell Biol* **19**, 174-179, doi:10.1016/j.tcb.2009.01.006 (2009).
41 Salbreux, G., Charras, G. & Paluch, E. Actin cortex mechanics and cellular morphogenesis. *Trends Cell Biol* **22**, 536-545, doi:10.1016/j.tcb.2012.07.001 (2012).
42 Rosa, A., Vlassaks, E., Pichaud, F. & Baum, B. Ect2/Pbl acts via Rho and polarity proteins to direct the assembly of an isotropic actomyosin cortex upon mitotic entry. *Dev Cell* **32**, 604-616, doi:10.1016/j.devcel.2015.01.012 (2015).

43 Ramanathan, S. P. *et al.* Cdk1-dependent mitotic enrichment of cortical myosin II promotes cell rounding against confinement. *Nat Cell Biol* **17**, 148-159, doi:10.1038/ncb3098 (2015).
44 Lambert, M. *et al.* Nucleation and growth of cadherin adhesions. *Exp Cell Res* **313**, 4025-4040, doi:10.1016/j.yexcr.2007.07.035 (2007).
45 Liu, Z. *et al.* Blebbistatin inhibits contraction and accelerates migration in mouse hepatic stellate cells. *Br J Pharmacol* **159**, 304-315, doi:10.1111/j.1476-5381.2009.00477.x (2010).
46 Konvalinka, J. *et al.* An active-site mutation in the human immunodeficiency virus type 1 proteinase (PR) causes reduced PR activity and loss of PR-mediated cytotoxicity without apparent effect on virus maturation and infectivity. *J Virol* **69**, 7180-7186 (1995).
47 Honer, B., Shoeman, R. L. & Traub, P. Human immunodeficiency virus type 1 protease microinjected into cultured human skin fibroblasts cleaves vimentin and affects cytoskeletal and nuclear architecture. *J Cell Sci* **100**, 799-807 (1991).
48 Sanghvi-Shah, R. & Weber, G. F. Intermediate Filaments at the Junction of Mechanotransduction, Migration, and Development. *Front Cell Develop Biol* **5**, 81, doi:10.3389/fcell.2017.00081 (2017).
49 Chou, Y. H., Opal, P., Quinlan, R. A. & Goldman, R. D. The relative roles of specific N- and C-terminal phosphorylation sites in the disassembly of intermediate filament in mitotic BHK-21 cells. *J Cell Sci* **109**, 817-826 (1996).
50 Meisen, W. H. *et al.* Changes in BAI1 and nestin expression are prognostic indicators for survival and metastases in breast cancer and provide opportunities for dual targeted therapies. *Mol Cancer Ther* **14**, 307-314, doi:10.1158/1535-7163.MCT-14-0659 (2015).
51 Leduc, C. & Etienne-Manneville, S. Regulation of microtubule-associated motors drives intermediate filament network polarization. *J Cell Biol* **216**, 1689-1703, doi:10.1083/jcb.201607045 (2017).
52 Esue, O., Carson, A. A., Tseng, Y. & Wirtz, D. A direct interaction between actin and vimentin filaments mediated by the tail domain of vimentin. *J Biol Chem* **281**, 30393-30399, doi:10.1074/jbc.M605452200 (2006).
53 Cary, R. B. *et al.* Vimentin's tail interacts with actin-containing structures in vivo. *J Cell Sci* **107 (Pt 6)**, 1609-1622 (1994).
54 Huber, F., Boire, A., Lopez, M. P. & Koenderink, G. H. Cytoskeletal crosstalk: when three different personalities team up. *Curr Opin Cell Biol* **32**, 39-47, doi:10.1016/j.ceb.2014.10.005 (2015).
55 Robert, A., Herrmann, H., Davidson, M. W. & Gelfand, V. I. Microtubule-dependent transport of vimentin filament precursors is regulated by actin and by the concerted action of Rho- and p21-activated kinases. *FASEB J* **28**, 2879-2890, doi:10.1096/fj.14-250019 (2014).
56 Wiche, G. & Winter, L. Plectin isoforms as organizers of intermediate filament cytoarchitecture. *Bioarchitecture* **1**, 14-20, doi:10.4161/bioa.1.1.14630 (2011).
57 Foisner, R., Malecz, N., Dressel, N., Stadler, C. & Wiche, G. M-phase-specific phosphorylation and structural rearrangement of the cytoplasmic cross-linking protein plectin involve p34cdc2 kinase. *Mol Biol Cell* **7**, 273-288 (1996).
58 Spurny, R., Gregor, M., Castanon, M. J. & Wiche, G. Plectin deficiency affects precursor formation and dynamics of vimentin networks. *Exp Cell Res* **314**, 3570-3580, doi:10.1016/j.yexcr.2008.09.012 (2008).
59 Kouklis, P. D., Papamarcaki, T., Merdes, A. & Georgatos, S. D. A potential role for the COOH-terminal domain in the lateral packing of type III intermediate filaments. *J Cell Biol* **114**, 773-786 (1991).

60 Kornreich, M., Avinery, R., Malka-Gibor, E., Laser-Azogui, A. & Beck, R. Order and disorder in intermediate filament proteins. *FEBS Lett* **589**, 2464-2476, doi:10.1016/j.febslet.2015.07.024 (2015).

61 Sarria, A. J., Lieber, J. G., Nordeen, S. K. & Evans, R. M. The presence or absence of a vimentin-type intermediate filament network affects the shape of the nucleus in human SW-13 cells. *J Cell Sci* **107**, 1593-1607 (1994).

62 Stamatakis, K., Sánchez-Gómez, F. J. & Pérez-Sala, D. Identification of novel protein targets for modification by 15-deoxy-$\Delta^{12,14}$-prostaglandin J_2 in mesangial cells reveals multiple interactions with the cytoskeleton. *J Am Soc Nephrol* **17**, 89-98 (2006).

63 Ivorra, C. *et al.* A mechanism of AP-1 suppression through interaction of c-Fos with lamin A/C. *Genes Dev* **20**, 307-320 (2006).

64 Lindsten, K., Uhlikova, T., Konvalinka, J., Masucci, M. G. & Dantuma, N. P. Cell-based fluorescence assay for human immunodeficiency virus type 1 protease activity. *Antimicrob Agents Chemother* **45**, 2616-2622 (2001).

65 Viedma-Poyatos, A., de Pablo, Y., Pekny, M. & Pérez-Sala, D. The cysteine residue of glial fibrillary acidic protein is a critical target for lipoxidation and required for efficient network organization. *Free Rad Biol Med* **120,** 380-394, doi: 10.1016/j.freeradbiomed.2018.04.007 (2018).

66 Gharbi, S., Garzón, B., Gayarre, J., Timms, J. & Pérez-Sala, D. Study of protein targets for covalent modification by the antitumoral and anti-inflammatory prostaglandin PGA_1: focus on vimentin. *J Mass Spectrom* **42,** 1474-1484 (2007).

Figure legends:

Fig. 1. **Assembly of tailless vimentin (1-411) in several cell types.** (A) Scheme of vimentin showing the various domains. Numbers in boxes depict the coils of the rod; the sequence of the tail domain is displayed in full. (B) SW13/cl.2 (upper panels) or MCF7 cells (lower panels) were transfected with the indicated constructs and observed live 48 h later. (C) SW13/cl.2 cells were transfected with different proportions of constructs coding for vimentin wild type (wt) or tailless (1-411), as indicated in the lower panel. The condensation of vimentin was measured as the area occupied by vimentin (green fluorescence) with respect to the total cellular area (red background). The histogram shows average values ± SEM of twenty determinations. *$p<0.05$ by Student's *t*-test. (D) U373-MG astrocytoma cells in p35 dishes were transfected with 2 μg of RFP//vimentin wt or (1-411), and the distribution of endogenous vimentin was assessed by immunofluorescence with V9 anti-vimentin antibody (green). Endogenous vimentin condensation was estimated as the ratio between the area of the green signal and the total cell area (red). The histogram shows average values ± SEM of twenty determinations. *$p<0.001$ by Student's *t*-test.

Fig. 2. **Tailless vimentin closely associates with nuclei in resting cells and interferes with chromosomes in mitosis.** (A) Single overlay sections of immunofluorescence assays carried out on SW13/cl.2 cells transfected with RFP//vimentin wt or (1-411) alone (left panels) or in combination with CFP-lamin A (middle panels). Live cell visualization was performed upon transfection with CFP-lamin A plus GFP-vim wt or (1-411) (right panels). Where indicated, nuclei were counterstained with DAPI. Insets display overall projections showing also the RFP background (middle and left panels) and/or the individual channels (right panels). (B) Cells were transfected with RFP//vimentin wt or (1-411) and vimentin distribution in mitosis was observed by immunofluorescence. A monoclonal antibody recognizing the N-terminus of vimentin was used for these experiments. Single sections taken at mid-cell height (left and middle panels) and 3D projections (right panels) are shown. Small panels below each image depict overall projections for vimentin alone (left) or for the three channels (vimentin, RFP and DAPI).

Fig. 3. **Live cell monitoring of cells expressing vimentin wt or (1-411) during mitosis.** SW13/cl.2 cells were transfected with RFP//vimentin plus GFP-vimentin wt or (1-411), as indicated, for live cell monitoring. Several fields were randomly selected and images were acquired every 15 min. Representative images of the overlays of DIC and green fluorescence at the indicated time points are shown.

Fig. 4. **Interaction of vimentin wt and (1-411) with microtubules and actin filaments.** The distribution of vimentin and tubulin or actin was assessed in resting (images on the left for all experimental conditions) and mitotic cells (images on the right). A) SW13/cl.2 cells transfected with RFP//vimentin wt or (1-411) were treated in the absence or presence of 5 μM nocodazole for 30 min in serum-free medium. Vimentin (green) and tubulin (red) were visualized by immunofluorescence. (B) SW13 cells were transfected as above and fixed. F-actin was stained with Phalloidin (red). Fluorescence intensity profiles of vimentin and actin along the dotted lines are shown in the right panels. (C) The distribution of f-actin and vimentin in resting and mitotic cells was assessed in several cell types expressing endogenous (U373-MG, BAEC,

human dermal fibroblasts) or transfected (MCF7) vimentin. Enlarged areas of the cell periphery showing the distribution of vimentin are depicted in insets. Nuclei were counterstained with DAPI. Single sections at mid-cell height are shown in all panels. Single channel images are shown in Suppl. Fig. S.

Fig. 5. **Analysis of the relative positions of vimentin and actin in mitosis by superresolution microscopy.** SW13/cl.2 cells stably transfected with RFP//vimentin wt were treated with 0.4 μM nocodazole overnight. Vimentin was detected by immunofluorescence with Alexa488-conjugated V9 antibody and actin was stained with TRITC-Phalloidin. (A) STED images of several cells are shown. Colocalization analysis was performed with Leica software. Numbers in insets represent the Pearson's coefficient and the percentage of colocalization for the whole cell or for the regions enlarged, as indicated. (B) 3D reconstruction of vimentin organization, after deconvolution of the green channel using Imaris software, for one representative cell. (C) 3D reconstruction using the basal half of the sections from the same cell in order to show the "inside" and the "outside" of the sphere. The semi-sphere edge is marked (dotted line) and points of putative vimentin protrusion into the actin cortex are indicated by arrows.

Fig. 6. **Effect of f-actin disruption on the organization of vimentin in mitosis.** (A) SW13/cl.2 cells transfected with RFP//vimentin wt or (1-411) were cultured in the absence or presence of 10 μg/ml cytochalasin B for 30 min in serum-free medium. Vimentin and f-actin were detected as above and their fluorescence intensity profiles along the dotted lines are shown in the right panels. For (A), (B) and (C), left panels show resting cells and right panels, mitotic cells. (B) Cells transfected with RFP//vimentin wt were treated in serum-free medium with 2.5 μM latrunculin A for 30 min, 2 μg/ml C3 toxin for 3 h, or 20 μM blebbistatin for 1 h, as indicated, and processed by immunofluorescence. Images of single sections taken at mid-height of resting and dividing cells are shown. (C) Cells expressing RFP//vimentin wt were treated with electrophilic lipids, 10 μM HNE 4 h, 20 μM PGA_1 for 20 h, and processed as above. The histogram shows average values ± SEM from 15 determinations of the proportion of central versus total vimentin cellular fluorescence, as an index of the impairment of peripheral localization. The values corresponding to tailless vimentin (1-411) are included here for comparison. (D) SW13/cl.2 cells were transfected with a combination of RFP//vimentin wt (80%) plus mCherry-vimentin wt (20%) and vimentin filaments (red) were monitored in live cells. In addition, cells were transfected with GFP-PR, coding the HIV-type I protease, and the corresponding green fluorescence is depicted in insets. In upper panels, cells were imaged 24 h after transfection. In the lower panels, the HIV inhibitor ritonavir was added immediately after transfection and cells were imaged 24 h later (left panel). Note the more intense GFP fluorescence indicative of the inhibition of GFP-PR autolysis. Subsequently, ritonavir was removed and cells were imaged 5 h later (right panel). (E) At the end of the experiment, cells were fixed and stained with DAPI to identify mitotic cells. Vimentin is artificially colored in green.

Fig. 7. **Organization and mitotic distribution of several C-terminal truncated vimentin mutants.** (A) Sequence of the various vimentin truncated mutants used in this study. (B) Overall projections of live SW13/cl.2 or MCF7 cells transfected with a combination of RFP//vimentin(1-423) plus GFP-vimentin(1-423). Insets depict the overlay with the background red fluorescence to show the cell contour. (C) SW13/cl.2 cells were transfected with

RFP//vimentin(1-423) and the distribution of the truncated vimentin in mitotic cells assessed by immunofluorescence. Nuclei were counterstained with DAPI. A representative single section at mid-cell height (left) and a 3D projection (right) are shown. Lower panels show the overall projections of the green (vimentin) channel alone or of the overlay of vimentin, DAPI and the red background fluorescence. (D) Live cells transfected with RFP//vimentin(1-423) plus GFP-vimentin(1-423) were monitored by time-lapse microscopy. Representative cases of asymmetric partition of vimentin (upper panels) and mitotic catastrophe (lower panels) are shown. (E) Cells were transfected as in (C) and the distribution of vimentin and f-actin was monitored in resting and mitotic cells. Images are single sections at mid-cell height. (F and J) Cells were transfected with RFP//vimentin (1-448) in (F), or (1-459) in (J), alone or in combination with the corresponding GFP fusion construct, as indicated, and vimentin distribution was monitored by immunofluorescence (left panels) or direct visualization of live cells (right panels). (G and K) Cells transfected with RFP//vimentin(1-448) in (G), or (1-459) in (K) were analyzed as in (C). (H and L) Cells transfected with RFP//vimentin(1-448) in (H), or (1-459) in (L) were monitored live and representative sequences are shown. In (H), an uncomplete division ending in cell death (upper panel) and an asymmetric division (lower panel) are shown. In (L), a normal division (upper panel) and an asymmetric division (lower panel) are shown. (I and M) The distribution of vimentin and f-actin in cells transfected with RFP//vimentin(1-448) (I) or RFP//vimentin(1-459) (M) is shown.

Fig. 8. **Assembly and distribution of GFP fusion constructs of truncated forms of vimentin.** (A) SW13/cl.2 cells transfected with the constructs shown in panel (D) and 48 h after transfection the morphology of the assemblies formed was assessed by live confocal microscopy. Overall projections are shown. Insets show enlarged areas of interest. The histogram (right) depicts the percentage of cells with squiggles or short filaments for every construct. Results are average values ± SEM of at least 15 determinations from several experiments totaling at least 100 cells per experimental condition.*$p<0.05$ by Student's *t*-test. (B) Cells were transfected with the indicated constructs, fixed, and the distribution of vimentin and f-actin assessed as above. Both interphase (left images) and mitotic cells (right images) are shown. Where indicated, cells were treated overnight with 0.4 μM nocodazole (+noc) in complete medium to increase the proportion of mitotic cells. Nuclei were counterstained with DAPI. Single sections taken at mid-cell height are shown in all cases. The fluorescence intensity profiles for vimentin and f-actin along the dotted lines are shown on the right for every condition. (C) The histogram shows the proportion of dots associated with the cell periphery for every construct. In this case, GFP-vimentin C328S, which contains the tail domain, is used as a control. GFP-vimentin(1-459) is excluded from this graph due to its organization mainly in squiggles or short filaments. Results are average values of at least 10 fields from at least three experiments per condition. *$p<0.01$ vs GFP-vimentin C328S; #$p<0.001$ vs GFP-vimentin(1-448). (D) Scheme illustrating the sequence of the various GFP-vimentin truncated constructs.

Fig. 9. **Schematic representation of the distribution of vimentin wt and tailless (1-411) in dividing cells.** In certain cell types in which vimentin filaments persist in mitosis, vimentin localizes to the mitotic cortex, intertwining with cortical actin. This organization is perturbed in tailless vimentin, resulting in the accumulation of vimentin bundles close to the mitotic spindle and dividing chromosomes, which associates with severe alterations in the progression of mitosis, including asymmetric partitions and mitotic catastrophes.

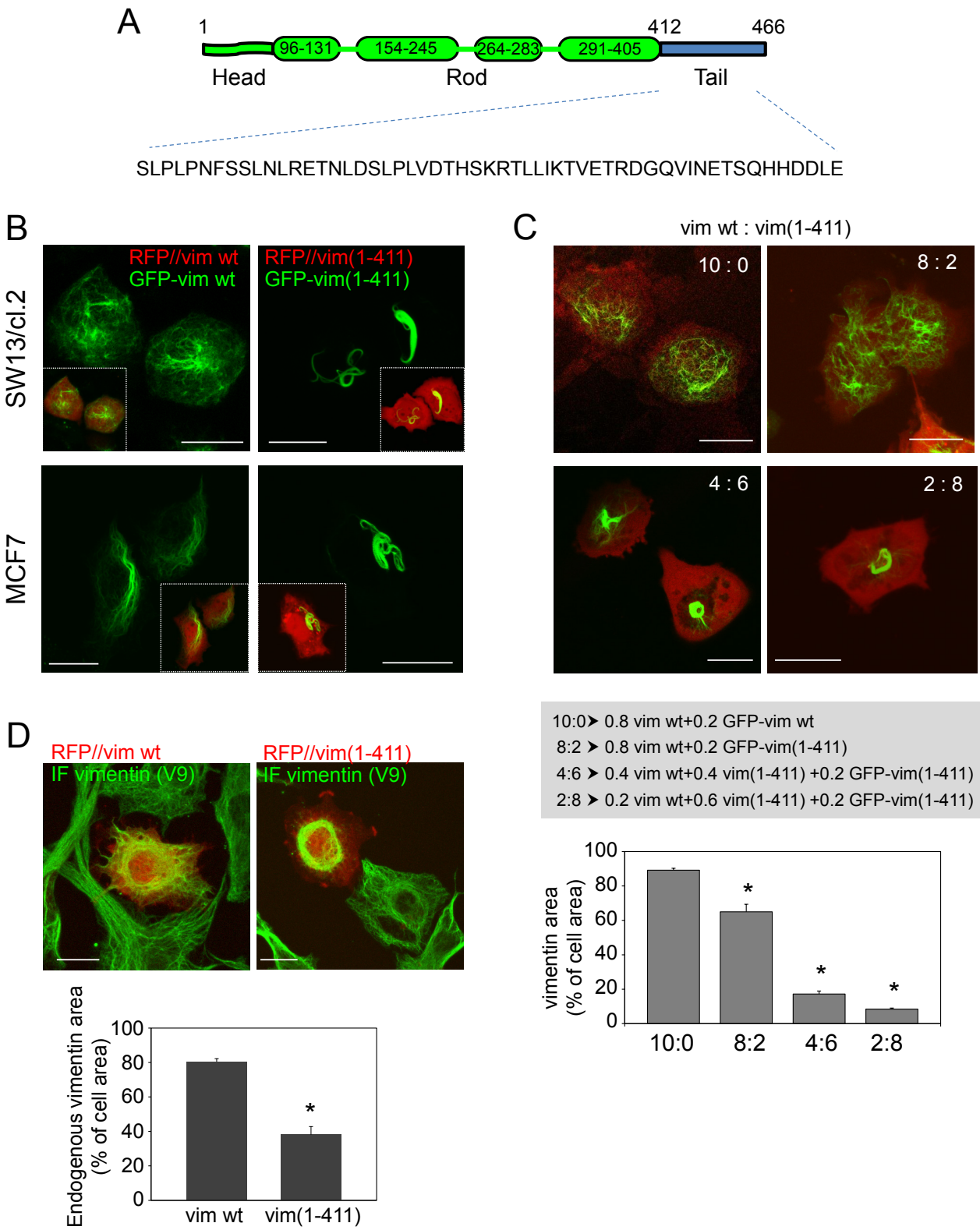
A
1
412
466
96-131
154-245
264-283
291-405
Head
Rod
Tail
SLPLPNFSSLNLRETNLDSLPLVDTHSKRTLLIKTVETRDGQVINETSQHHDDLE
B
SW13/cl.2
MCF7
RFP//vim wt
GFP-vim wt
RFP//vim(1-411)
GFP-vim(1-411)
C
vim wt : vim(1-411)
10 : 0
8 : 2
4 : 6
2 : 8
D
RFP//vim wt
IF vimentin (V9)
RFP//vim(1-411)
IF vimentin (V9)
Endogenous vimentin area
(% of cell area)
100
80
60
40
20
0
vim wt
vim(1-411)
10:0 ➤ 0.8 vim wt+0.2 GFP-vim wt
8:2 ➤ 0.8 vim wt+0.2 GFP-vim(1-411)
4:6 ➤ 0.4 vim wt+0.4 vim(1-411) +0.2 GFP-vim(1-411)
2:8 ➤ 0.2 vim wt+0.6 vim(1-411) +0.2 GFP-vim(1-411)
vimentin area
(% of cell area)
10:0
8:2
4:6
2:8

Figure 1

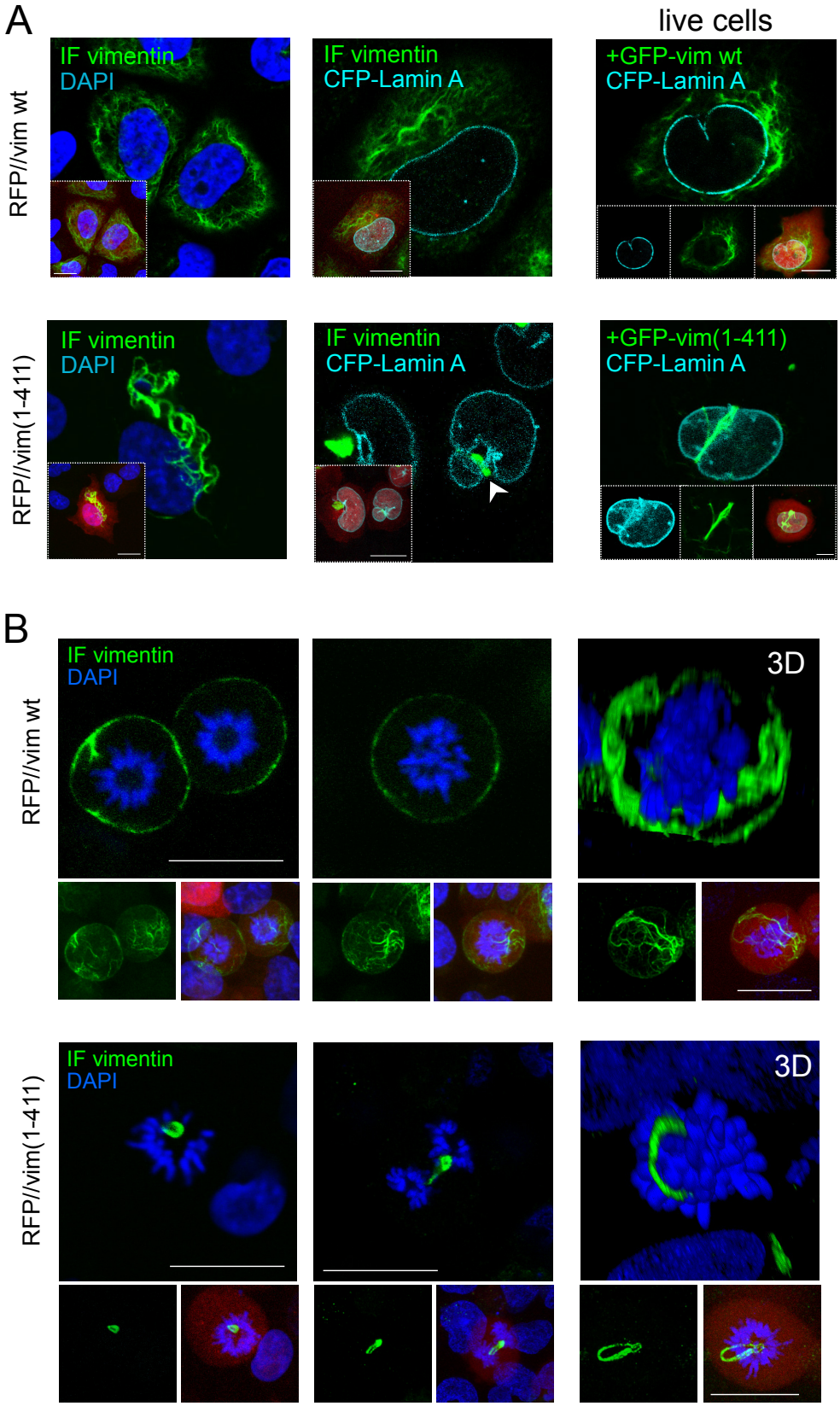
A
live cells
RFP//vim wt
IF vimentin
DAPI
IF vimentin
CFP-Lamin A
+GFP-vim wt
CFP-Lamin A
RFP//vim(1-411)
IF vimentin
DAPI
IF vimentin
CFP-Lamin A
+GFP-vim(1-411)
CFP-Lamin A
B
RFP//vim wt
IF vimentin
DAPI
3D
RFP//vim(1-411)
IF vimentin
DAPI
3D

Figure 2

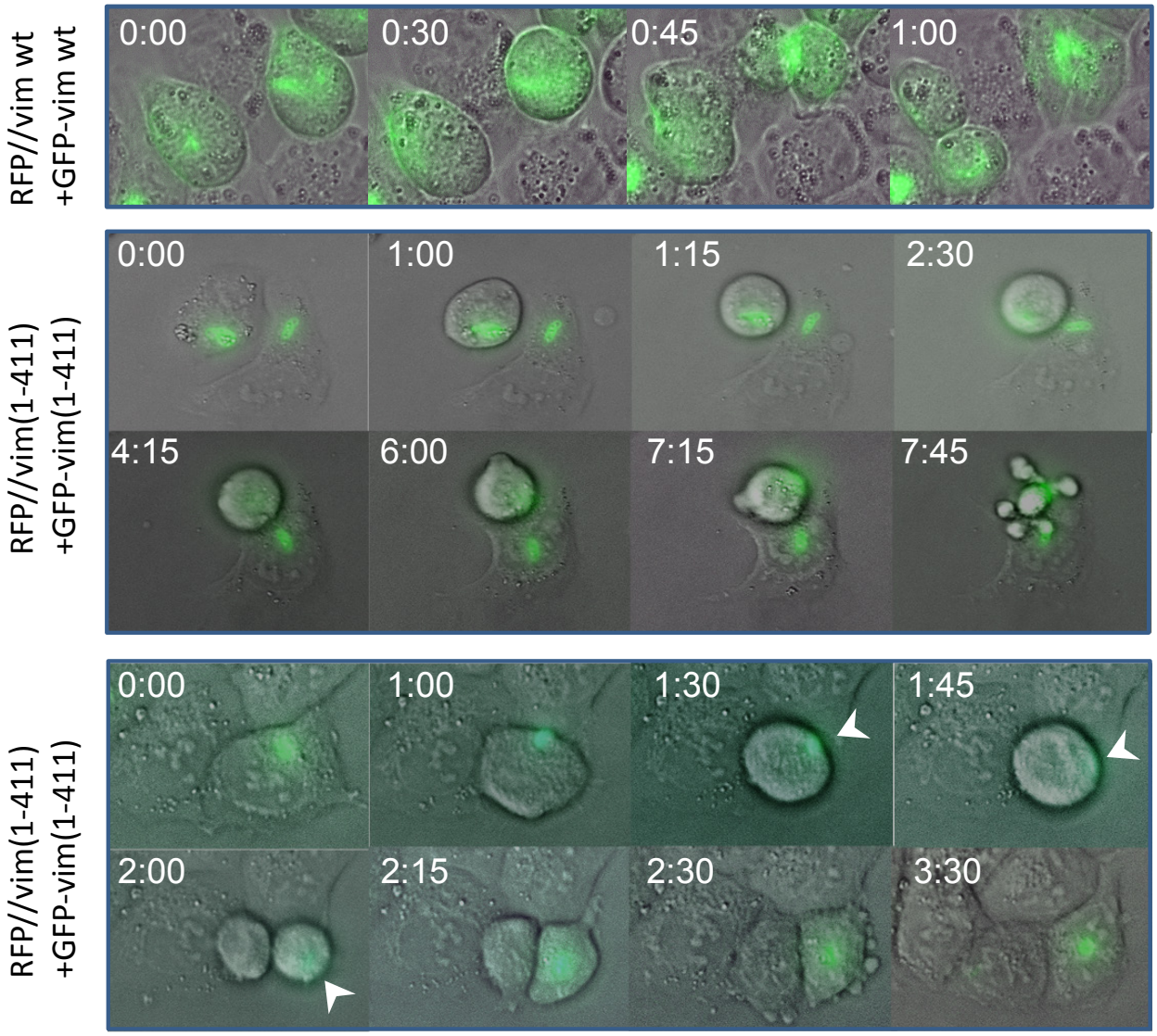
RFP//vim wt
+GFP-vim wt
0:00
0:30
0:45
1:00
RFP//vim(1-411)
+GFP-vim(1-411)
0:00
1:00
1:15
2:30
4:15
6:00
7:15
7:45
RFP//vim(1-411)
+GFP-vim(1-411)
0:00
1:00
1:30
1:45
2:00
2:15
2:30
3:30

Figure 3

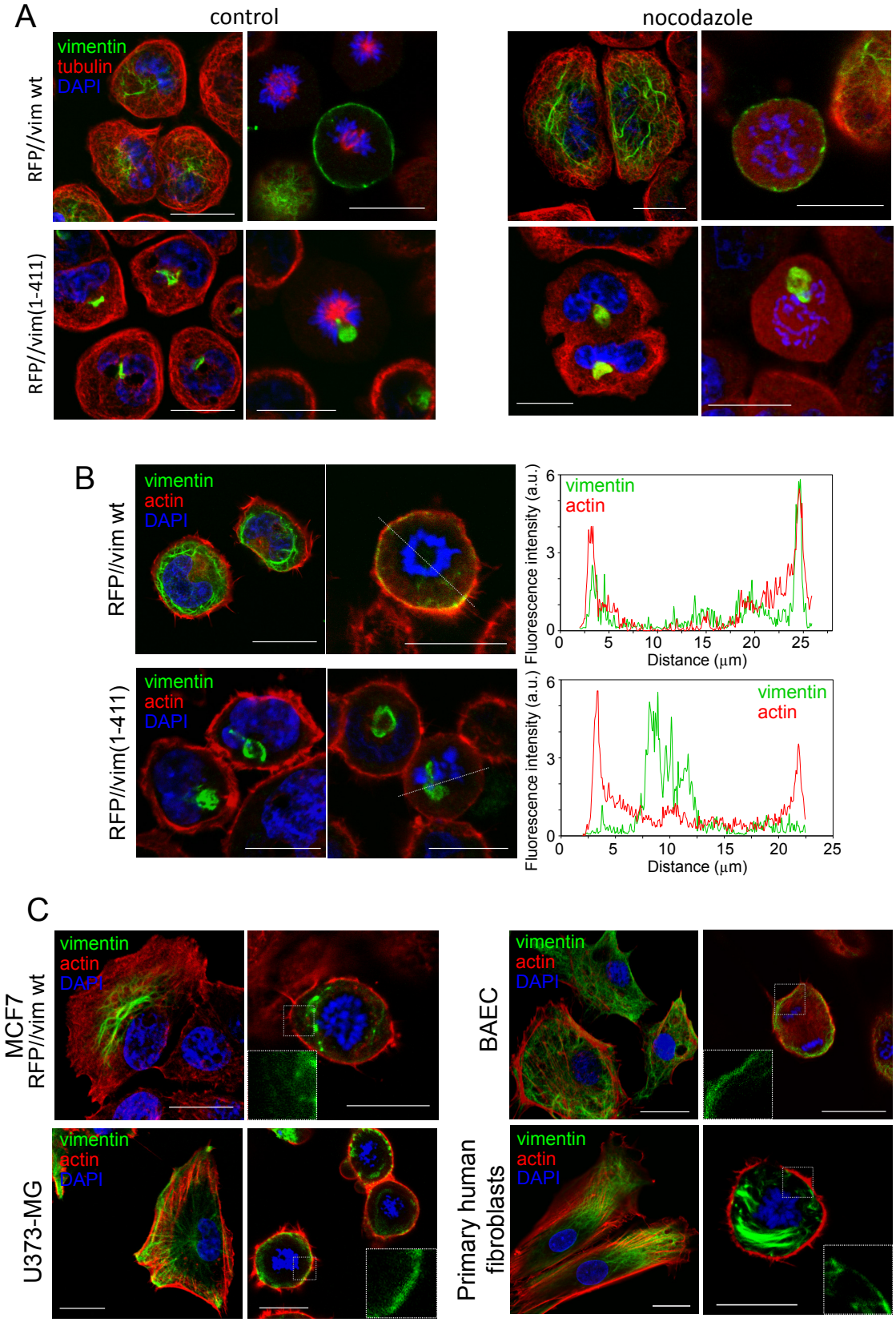
A
control
nocodazole
vimentin
tubulin
DAPI
RFP//vim wt
RFP//vim(1-411)
B
vimentin
actin
DAPI
RFP//vim wt
RFP//vim(1-411)
Fluorescence intensity (a.u.)
Distance (μm)
C
MCF7
RFP//vim wt
BAEC
U373-MG
Primary human fibroblasts

Figure 4

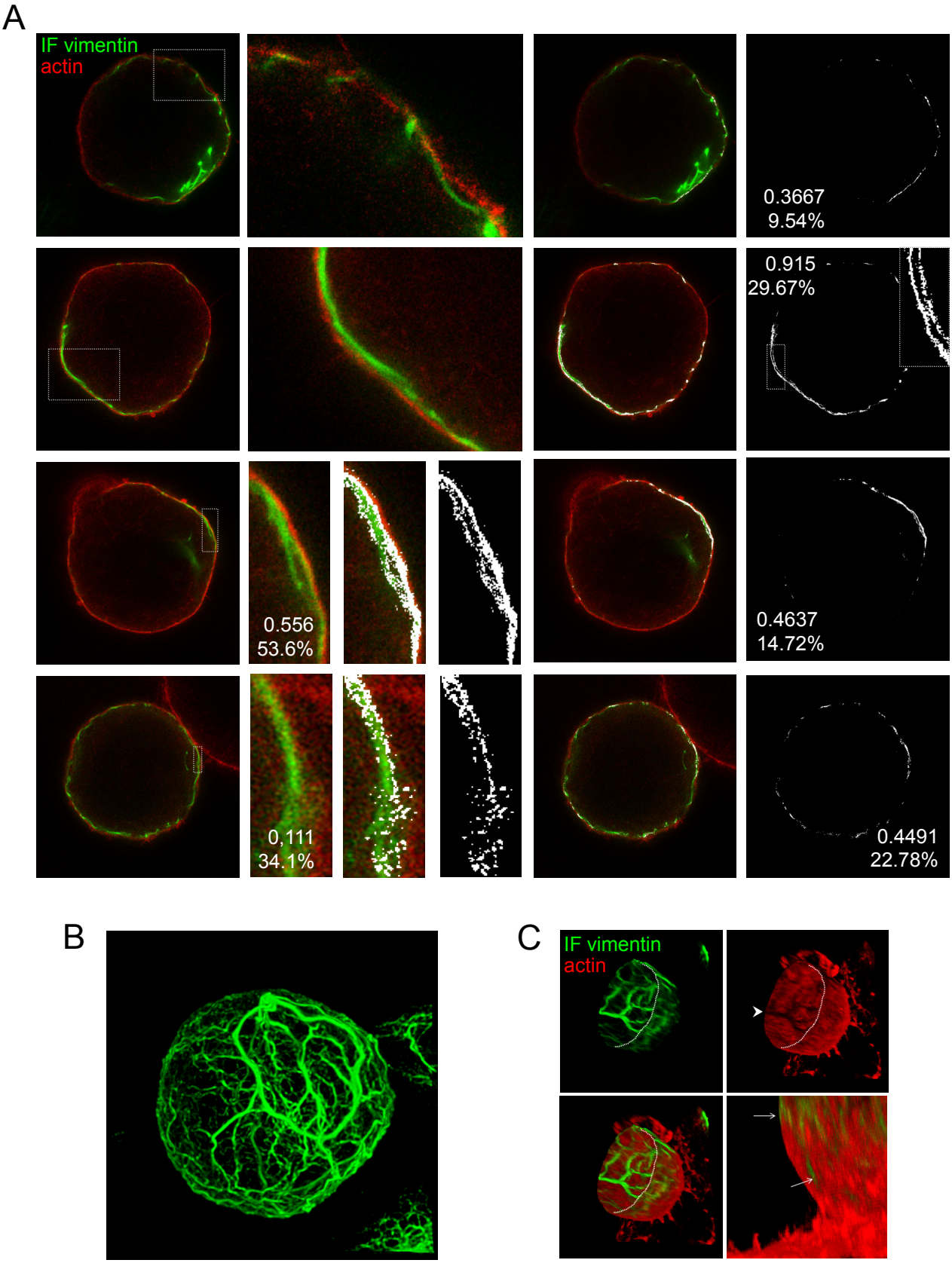
A
IF vimentin
actin
0.3667
9.54%
0.915
29.67%
0.556
53.6%
0.4637
14.72%
0,111
34.1%
0.4491
22.78%
B
C
IF vimentin
actin

Figure 5

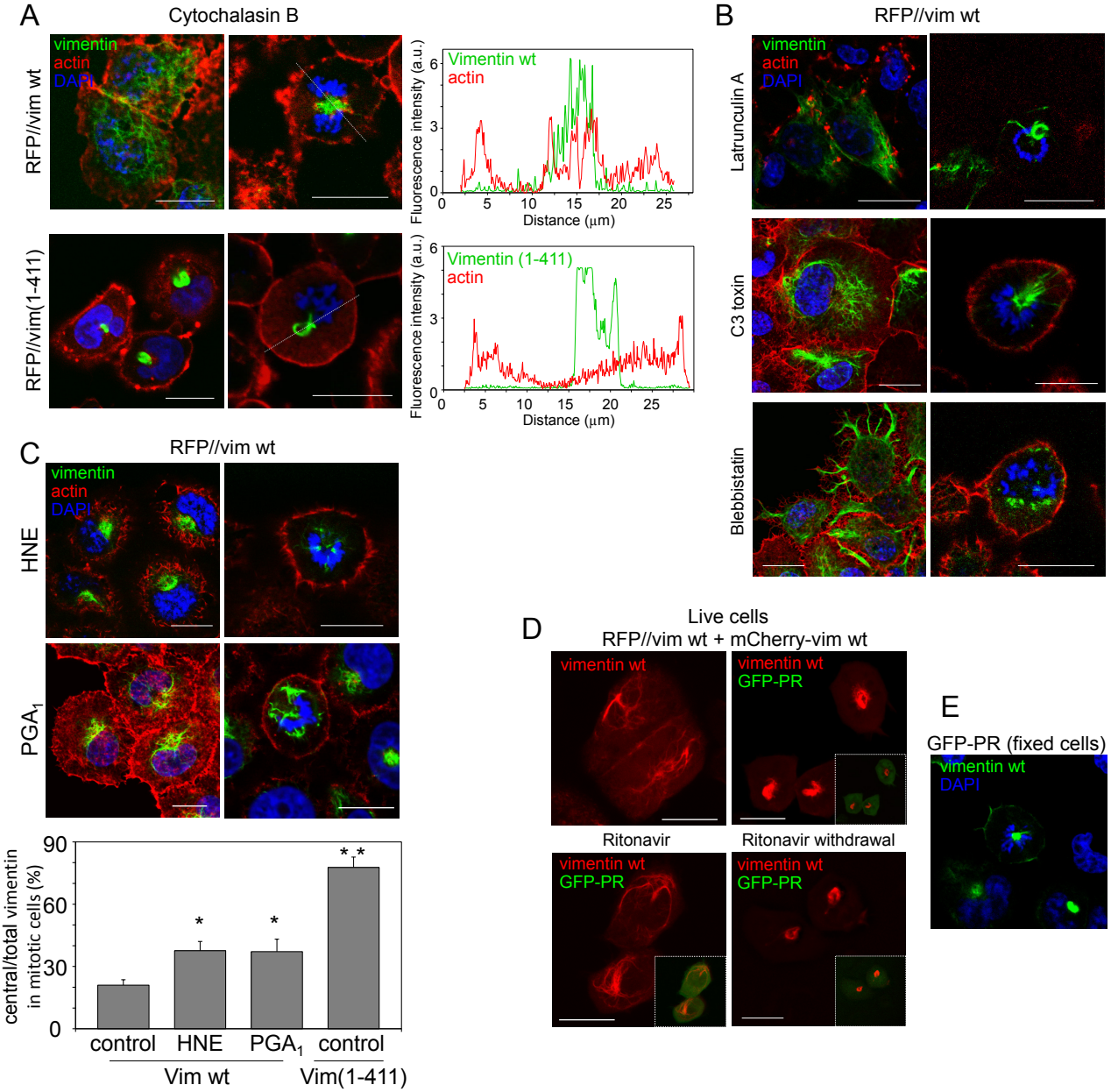
A
Cytochalasin B
RFP//vim wt
vimentin
actin
DAPI
Vimentin wt
actin
Fluorescence intensity (a.u.)
Distance (μm)
RFP//vim(1-411)
Vimentin (1-411)
B
RFP//vim wt
Latrunculin A
C3 toxin
Blebbistatin
C
RFP//vim wt
HNE
PGA1
central/total vimentin in mitotic cells (%)
control
HNE
PGA1
control
Vim wt
Vim(1-411)
D
Live cells
RFP//vim wt + mCherry-vim wt
vimentin wt
GFP-PR
Ritonavir
Ritonavir withdrawal
E
GFP-PR (fixed cells)

Figure 6

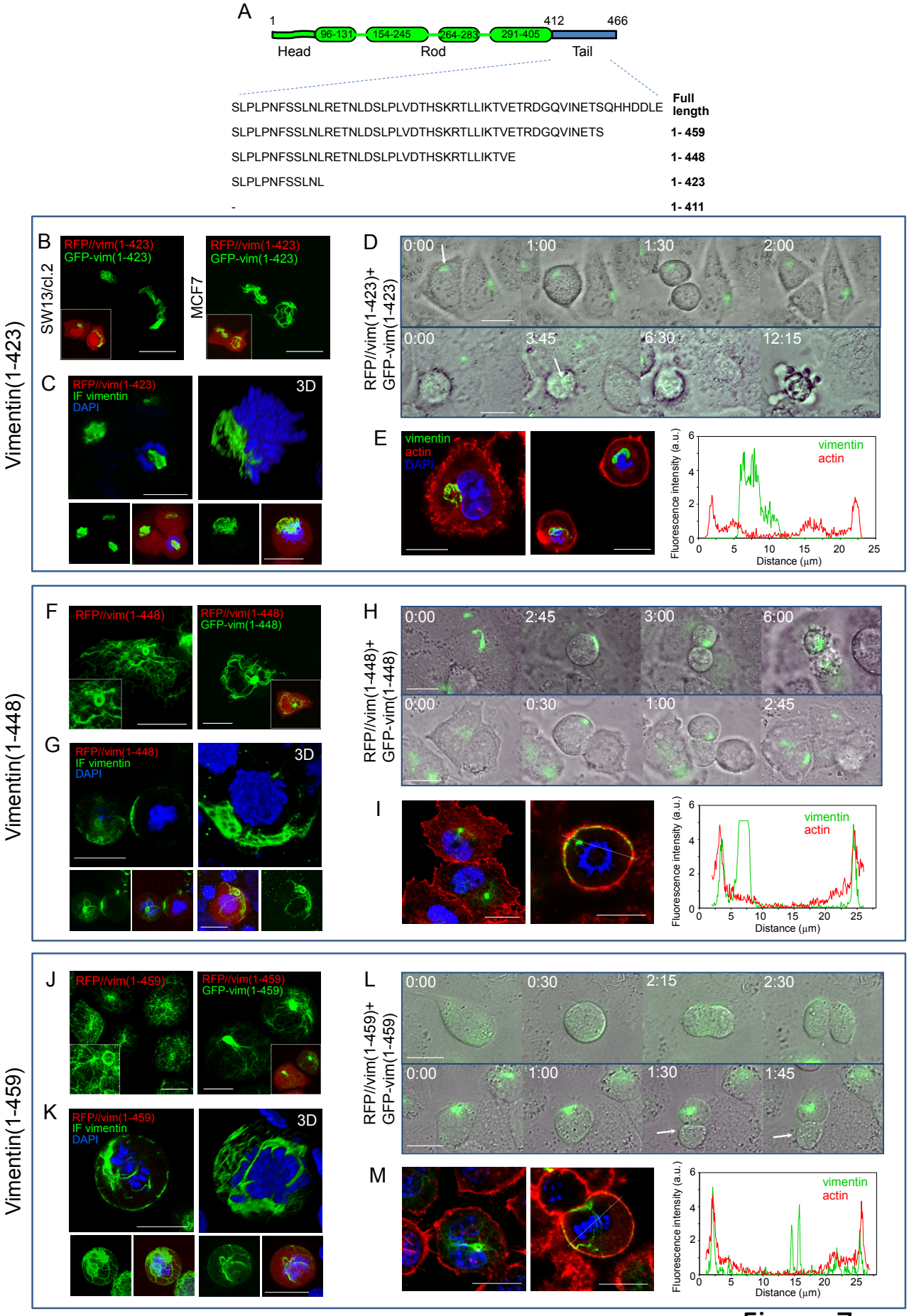
A
1
412
466
96-131
154-245
264-283
291-405
Head
Rod
Tail
SLPLPNFSSLNLRETNLDSLPLVDTHSKRTLLIKTVETRDGQVINETSQHHDDLE
Full length
SLPLPNFSSLNLRETNLDSLPLVDTHSKRTLLIKTVETRDGQVINETS
1- 459
SLPLPNFSSLNLRETNLDSLPLVDTHSKRTLLIKTVE
1- 448
SLPLPNFSSLNL
1- 423
-
1- 411
Vimentin(1-423)
B
SW13/cl.2
RFP//vim(1-423)
GFP-vim(1-423)
MCF7
RFP//vim(1-423)
GFP-vim(1-423)
C
RFP//vim(1-423)
IF vimentin
DAPI
3D
D
RFP//vim(1-423)+
GFP-vim(1-423)
0:00
1:00
1:30
2:00
0:00
3:45
6:30
12:15
E
vimentin
actin
DAPI
vimentin
actin
Fluorescence intensity (a.u.)
Distance (μm)
Vimentin(1-448)
F
RFP//vim(1-448)
RFP//vim(1-448)
GFP-vim(1-448)
G
RFP//vim(1-448)
IF vimentin
DAPI
3D
H
RFP//vim(1-448)+
GFP-vim(1-448)
0:00
2:45
3:00
6:00
0:00
0:30
1:00
2:45
I
vimentin
actin
Fluorescence intensity (a.u.)
Distance (μm)
Vimentin(1-459)
J
RFP//vim(1-459)
RFP//vim(1-459)
GFP-vim(1-459)
K
RFP//vim(1-459)
IF vimentin
DAPI
3D
L
RFP//vim(1-459)+
GFP-vim(1-459)
0:00
0:30
2:15
2:30
0:00
1:00
1:30
1:45
M
vimentin
actin
Fluorescence intensity (a.u.)
Distance (μm)

Figure 7

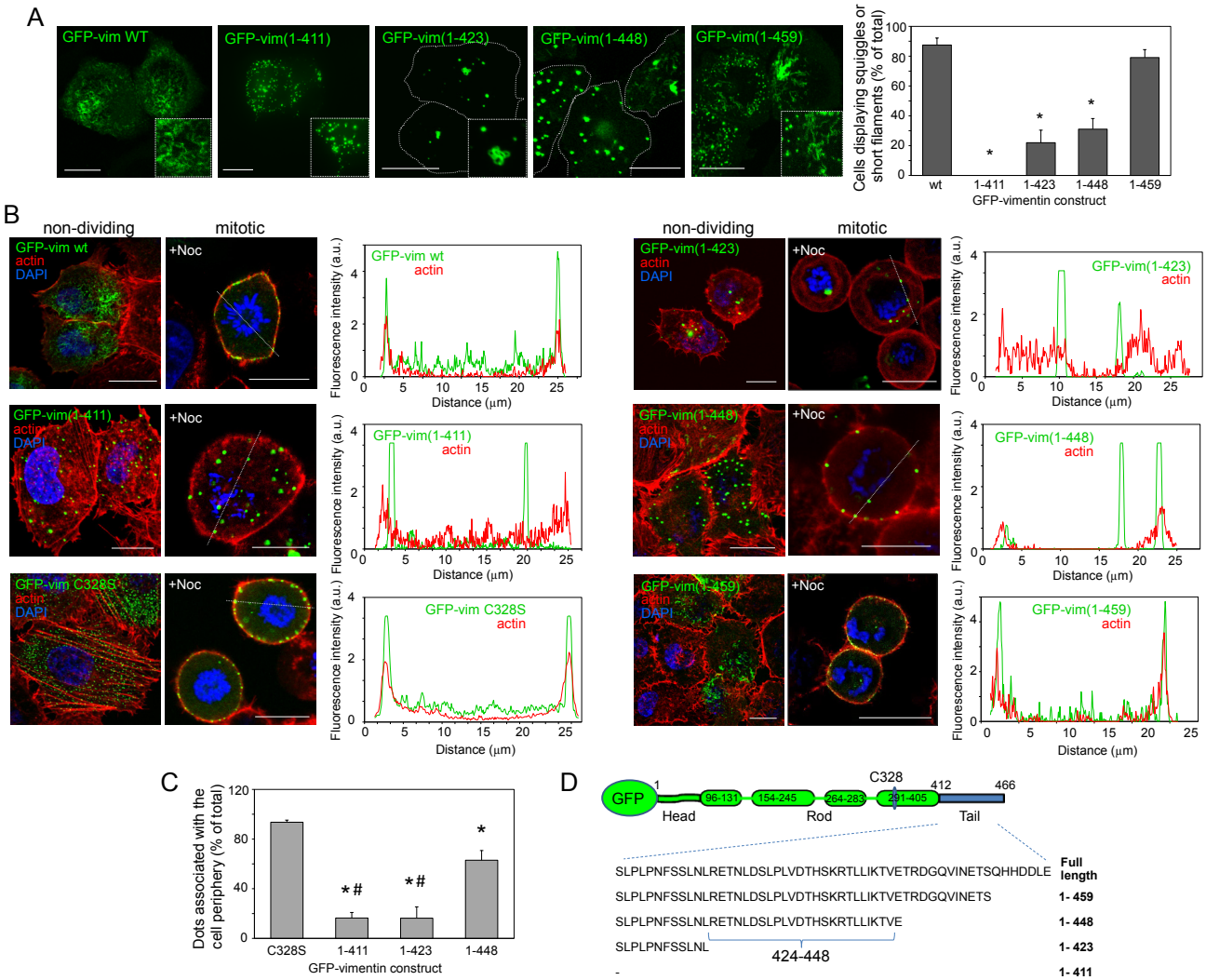
A
GFP-vim WT
GFP-vim(1-411)
GFP-vim(1-423)
GFP-vim(1-448)
GFP-vim(1-459)
Cells displaying squiggles or short filaments (% of total)
wt
1-411
1-423
1-448
1-459
GFP-vimentin construct
B
non-dividing
mitotic
GFP-vim wt
actin
DAPI
+Noc
GFP-vim(1-411)
GFP-vim C328S
GFP-vim(1-423)
GFP-vim(1-448)
GFP-vim(1-459)
Fluorescence intensity (a.u.)
Distance (μm)
C
Dots associated with the cell periphery (% of total)
C328S
1-411
1-423
1-448
GFP-vimentin construct
D
GFP
C328
Head
Rod
Tail
96-131
154-245
264-283
291-405
SLPLPNFSSLNLRETNLDSLPLVDTHSKRTLLIKTVETRDGQVINETSQHHDDLE
SLPLPNFSSLNLRETNLDSLPLVDTHSKRTLLIKTVETRDGQVINETS
SLPLPNFSSLNLRETNLDSLPLVDTHSKRTLLIKTVE
SLPLPNFSSLNL
424-448
Full length
1- 459
1- 448
1- 423
1- 411

Figure 8

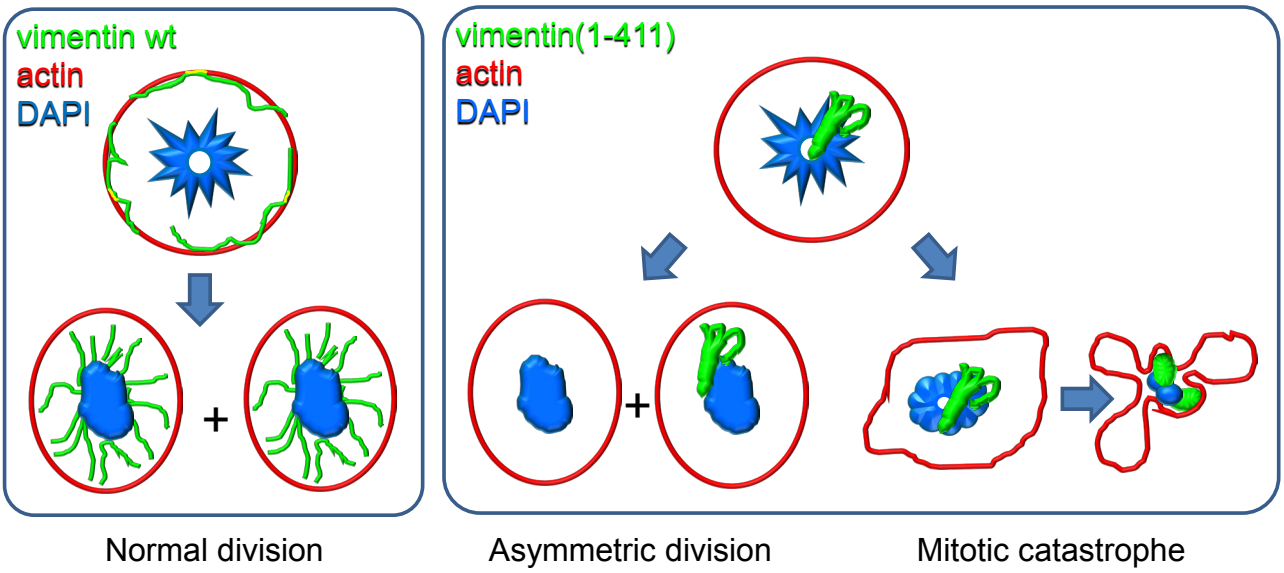
vimentin wt
actin
DAPI
+
vimentin(1-411)
actin
DAPI
+
Normal division
Asymmetric division
Mitotic catastrophe

Figure 9